CRK2 and C-terminal phosphorylation of NADPH oxidase RBOHD regulate ROS production in Arabidopsis

Running title: CRK2 in plant immune signaling

Key words: Cysteine-rich receptor-like kinase, reactive oxygen species, NADPH oxidase, phosphorylation, Arabidopsis

Sachie Kimura[1], Kerri Hunter[1], Lauri Vaahtera[2], Huy Cuong Tran[1#], Aleksia Vaattovaara[1], Anne Rokka[3], Sara Christina Stolze[4], Anne Harzen[4], Lena Meißner[1$], Maya Wilkens[1$], Thorsten Hamann[2], Masatsugu Toyota[5,6], Hirofumi Nakagami[4], Michael Wrzaczek[1*]

[1]Organismal and Evolutionary Biology Research Programme, Viikki Plant Science Centre, Faculty of Biological and Environmental Sciences, University of Helsinki, Helsinki, FI-00014, Finland.
[2]Department of Biology, Norwegian University of Science and Technology, 7491 Trondheim, Norway.
[3]Turku Centre for Biotechnology, University of Turku and Åbo Akademi, FI-20520, Finland.
[4] Protein Mass Spectrometry Group, Max-Planck Institute for Plant Breeding Research, Carl-von-Linné-Weg 10, D-50829 Cologne, Germany.
[5]Department of Biochemistry and Molecular Biology, Saitama University, Saitama 338-8570, Japan.
[6]Department of Botany, University of Wisconsin, Madison, WI, 53593, USA.
[#]Present address: Department of Biology, Lund University, Sölvegatan 35, 223 62 Lund, Sweden.
[$]Present address: Technische Universität Braunschweig, Germany.

* To whom correspondence should be addressed:
Michael Wrzaczek
Organismal and Evolutionary Biology Research Programme
Viikki Plant Science Centre, VIPS
Faculty of Biological and Environmental Sciences
Viikinkaari 1, PO Box 65
FIN-00014 Helsinki University
Finland
Email: michael.wrzaczek@helsinki.fi
Phone: +358 2941 57 773

ORCID IDs: 0000-0001-5736-2123 (SK), 0000-0002-2285-6999 (KH), 0000-0003-4733-4430 (LV), 0000-0002-7670-2215 (CT), 0000-0003-3452-0947 (AV), 0000-0003-1482-9154 (AR), 0000-0002-1421-9703 (SCR), 0000-0002-8605-6026 (LM), 0000-0003-4631-6177 (MWi), 0000-0001-8460-5151 (TH), 0000-0002-9544-0978 (MT), 0000-0003-2569-7062 (HN), 0000-0002-5946-9060 (MWr)

Abstract

Reactive oxygen species (ROS) are important messengers in eukaryotic organisms and their production is tightly controlled. Active extracellular ROS production by NADPH oxidases in plants is triggered by receptor-like protein kinase (RLK)-dependent signaling networks. Here we show that the cysteine-rich RLK CRK2 kinase activity is required for plant growth and CRK2 exists in a preformed complex with the NADPH oxidase RBOHD in Arabidopsis. Functional CRK2 is required for the full elicitor-induced ROS burst and consequently the *crk2* mutant is impaired in defense against the bacterial pathogen *Pseudomonas syringae pv.* tomato DC3000. Our work demonstrates that CRK2 regulates plant innate immunity. We identified *in vitro* CRK2-dependent phosphorylation sites in the C-terminal region of RBOHD. Phosphorylation of S703 RBOHD is enhanced upon flg22 treatment and substitution of S703 with alanine reduced ROS production in Arabidopsis. Phylogenetic analysis suggests that phospho-sites in C-terminal region of RBOHD are conserved throughout the plant lineage and between animals and plants. We propose that regulation of NADPH oxidase activity by phosphorylation of the C-terminal region might be an ancient mechanism.

Introduction

Plants are continuously confronted with stimuli from the surrounding environment, including abiotic cues and invading pathogens. Plant cells also perceive a plethora of signals from neighboring cells and distant tissues. Numerous plasma membrane proteins are involved in the meticulous monitoring and transduction of signals for inter- and intracellular communication. A common early feature of many cellular responses to various environmental changes involves the production of reactive oxygen species (ROS) (Kimura et al., 2017; Waszczak et al., 2018). While ROS are an inevitable by-product of aerobic metabolism their unrestricted accumulation can have deleterious consequences (Waszczak et al., 2018), ROS are also ubiquitous signaling molecules in plants and animals alike (Suzuki et al., 2011; Waszczak et al., 2018). Eukaryotic cells produce ROS in several subcellular compartments as well as the extracellular space, in plants referred to as apoplast (Kimura et al., 2017; Waszczak et al., 2018). A major component in the production of extracellular ROS is the evolutionarily conserved NADPH oxidase (NOX) family (Kimura et al., 2017; Meitzler et al., 2014). NOX-dependent ROS production is involved in regulation of immune functions, cell growth and apoptosis in animals and plants (Jiménez-Quesada et al., 2016; Waszczak et al., 2018).

Plant NOXs, referred to as respiratory burst oxidase homologs (RBOHs), have been identified as homologs of phagocyte gp91^{phox}/NOX2, which contains six transmembrane helices and a C-terminal NADPH- and FAD-binding cytoplasmic region (Torres et al., 2002). Unlike gp91^{phox}/NOX2, RBOHs contains an additional N-terminal region with Ca^{2+}-binding EF-hands, similar to non-phagocytic NOXs, such as NOX5 (Suzuki et al., 2011). RBOH activity is strictly controlled to avoid damaging consequences of unrestricted ROS production (Suzuki et al., 2011). *Arabidopsis thaliana* (Arabidopsis) RBOHD is the best-characterized RBOH and is involved in biotic and abiotic stress responses (Lee et al., 2013; Lee et al., 2018; Torres et al., 2002). The N-terminal region of RBOHD is phosphorylated by a variety of protein kinases, including receptor-like cytoplasmic kinases (RLCKs; Dubiella et al., 2013; Han et al., 2019; Kadota et al., 2014; Kaya, Takeda et al., 2018; Kimura et al., 2012; Li et al., 2014; Ogasawara et al., 2008; Zhang et al., 2018), for example BOTRYTIS-INDUCED KINASE 1 (BIK1; (Kadota et al., 2014; Li et al., 2014). While previous research has suggested a predominant role of phosphorylation of the N-terminal region for regulation of RBOH, phosphorylation of the C-terminal region is important for the regulation of human gp91^{phox}/NOX2 and NOX5 (Jagnandan et al., 2007; Raad et al., 2009). NADPH- and FAD-binding sites in C-terminus are highly conserved in NOXs and RBOHs, but it is unclear whether the C-terminus of plant RBOHs could also be a target for regulation of the ROS producing activity.

Apoplastic RBOH-dependent ROS production is a common response to the activation of receptor-like protein kinase (RLK; Shiu & Bleecker, 2001) signaling, in particular following perception of microbe-associated molecular patterns (MAMPs) or damage-associated molecular patterns (DAMPs; Couto & Zipfel, 2016; Kimura et al., 2017). However, the role of the so-called ROS burst and its integration into RLK-

triggered signaling networks are as yet unclear (Kimura et al., 2017). A large group of RLKs in plants is formed by the cysteine-rich RLKs (CRKs; Vaattovaara et al., 2019). The extracellular region of CRKs harbors two copies of the domain of unknown function 26 (DUF26) but the molecular function of the CRK ectodomain remains unknown (Vaattovaara et al., 2019). CRKs have been linked to ROS signaling (Bourdais et al., 2015; Idänheimo et al., 2014; Yadeta et al., 2017; Yeh et al., 2015) and cell death (Bourdais et al., 2015; Yadeta et al., 2017) and are important signaling elements in plant development, biotic and abiotic stress responses (Acharya et al., 2007; Bourdais et al., 2015; Chen et al., 2004; Chern et al., 2016; Hunter et al., 2019; Idänheimo et al., 2014; Tanaka et al., 2012; Wrzaczek et al., 2010; Yadeta et al., 2017; Yeh et al., 2015).

Here we characterize the role of CRK2 in immune signaling in response to MAMP-perception. CRK2 exists in a pre-formed complex with RBOHD. CRK2 controls the activity of RBOHD and functional CRK2 is required for full MAMP-induced ROS production. Importantly, we show that CRK2 phosphorylates the C-terminal region of RBOHD and modulates the ROS-production activity of RBOHD *in vivo*. Our results lead us to propose a novel mechanism for the regulation of RBOHD activity through phosphorylation of the C-terminal region and highlight a critical role for CRK2 in the precise control of the ROS burst in response to biotic stress.

Results

CRK2 kinase activity is important for plant development

CRK2 has been previously implicated in stress responses and development in Arabidopsis (Bourdais et al., 2015). CRK2 is a typical CRK with N-terminal signal peptide, extracellular region containing two DUF26 domains, transmembrane region and intracellular protein kinase domain (Fig. 1a). The *crk2* mutant was smaller than wild type (Col-0) plants (Fig. 1b; Bourdais et al., 2015), and displayed significantly reduced fresh (Fig. 1c) and dry weight (Fig. S1a). Over-accumulation of the plant hormone salicylic acid (SA) often causes a reduction of plant size, but SA levels were not significantly different between *crk2* and wild type plants (Fig. S1b). Expression of YFP-tagged CRK2 under the control of the CRK2 promoter (*CRK2pro::CRK2-YFP*) in the *crk2* background restored plant growth (Figs. 1b, 1c and S1a). Substitution of the ATP-binding lysine (K) at position 353 with glutamic acid (E; $CRK2^{K353E}$) or the aspartic acid (D) at position 450 in the catalytic domain VIb (Stone & Walker, 1995) with asparagine (N; $CRK2^{D450N}$) abated the kinase activity of CRK2 *in vitro* (Hunter et al., 2019). Kinase dead $CRK2^{K353E}$-YFP or $CRK2^{D450N}$-YFP under control of the *CRK2* promoter displayed the same subcellular localization as wild type CRK2-YFP (Figs. S1c) but failed to restore the growth defect of *crk2* (Figs. 1b, 1c and S1a). In summary, our results show that CRK2 is important for proper plant growth and its kinase activity is crucial for this function.

CRK2 is required for MAMP-triggered responses and resistance to *Pseudomonas syringae* pv. tomato DC3000

Previous results suggested that ROS production triggered by flg22, a MAMP derived from bacterial flagella, is reduced in *crk2* (Bourdais et al., 2015). Therefore, we tested the role of CRK2 in MAMP-induced ROS production in detail. ROS production triggered by flg22 was reduced in *crk2* and reintroduction of CRK2-YFP into the mutant background restored ROS production to the same levels as in Col-0 (Fig. 2a). The flg22-induced ROS production in plants expressing $CRK2^{D450N}$-YFP was comparable to *crk2* (Fig. 2b). Transcriptional upregulation of flg22 responsive genes (*FRK1* and *NHL10*) showed that MAMP-perception was not impaired in *crk2* (Figs. S2a and S2b). To test whether the reduced response of *crk2* to flg22 was accompanied by altered pathogen susceptibility, we measured growth of the hemibiotrophic bacterial pathogen *Pseudomonas syringae* DC3000 pv. tomato (*P*to DC3000). The *crk2* mutant was significantly more susceptible to the virulent pathogen compared to Col-0 (Fig. 2c). CRK2-YFP but not the kinase-dead $CRK2^{D450N}$-YFP restored the pathogen susceptibility of *crk2* (Fig. 2c). ROS production induced by chitin (Fig. S2c) or pep1 (Fig. S2d) was also reduced in *crk2* compared to Col-0 suggesting that the reduced MAMP- or DAMP-triggered ROS production in *crk2* is a general response and not specific to flg22.

To investigate the role of CRK2 in flg22-triggered responses in more detail, we assessed Ca^{2+} signaling, MAPK activation and callose deposition in *crk2*. Application of flg22 resulted in a rapid increase in cytosolic Ca^{2+} ($[Ca^{2+}]_{cyto}$) levels in wild type plants, which express the FRET-based Ca^{2+}-sensor *YCNano-65* (Choi et al., 2014, Lenglet et al., 2017, Toyota et al., 2018). This response was strongly reduced in the *crk2* mutant background, *YCNano65/crk2* (Figs. S2e and S2f). Interestingly, flg22-dependent MAPK activation (Fig.

S2g) and callose deposition (Fig. S2h and S2i) were more pronounced in *crk2* compared to Col-0. Taken together, CRK2 is an essential component for mounting immune responses against the virulent bacterial pathogen in Arabidopsis, modulating extracellular ROS production, callose deposition, Ca^{2+} influx and MAPK activation.

CRK2 interacts with RBOHD and controls ROS production

RBOHD is the main source of MAMP/DAMP-induced extracellular ROS production (Couto & Zipfel, 2016; Kimura et al., 2017) and flg22-, pep1 and chitin-induced ROS production was significantly reduced in *crk2* (Figs. 2 and S2). RBOH proteins, including RBOHD, are synergistically activated by protein phosphorylation and Ca^{2+}-binding to EF-hand motifs in the N-terminal region (Kaya et al., 2018). Given the importance of the kinase activity of CRK2 in MAMP-induced ROS production we investigated whether CRK2 could activate RBOHD. To test this, we used human embryonic kidney 293T (HEK293T) cells, a human cell culture which produces minimal amounts of extracellular ROS due to a lack of expression of endogenous NADPH oxidases (Ogasawara et al., 2008). HEK293T cells were co-transfected with *3FLAG-RBOHD* and *CRK2-3Myc* or *3Myc-GFP* as control. Subsequently, RBOHD-mediated extracellular ROS production was measured by luminol-amplified chemiluminescence. Despite equal 3FLAG-RBOHD protein levels (Fig. S3a) ROS production in cells co-transfected with *CRK2-3Myc* and *3FLAG-RBOHD* was strongly elevated compared to cells co-transfected with *3FLAG-RBOHD* and *3Myc-GFP* (Fig. 3a). Co-transfection with the inactive variant *CRK2*^{D450N}*-3Myc* did not enhance ROS production by *3FLAG-RBOHD* compared to co-transfection with *CRK2-3Myc* (Fig. 3a). Transfection of *CRK2-3Myc* in the absence of *3FLAG-RBOHD* did not induce ROS production in HEK293T cells (Fig. 3a). Since RBOHD can also be activated by Ca^{2+}, HEK293T cells were treated with ionomycin, a Ca^{2+} ionophore that induces a rise in cytosolic Ca^{2+} levels. Ionomycin-induced transient ROS production (Δ_{delta} ROS: $ROS_{T=30}$ to $ROS_{T=31}$) in *CRK2-3Myc* and *3FLAG-RBOHD* co-transfected cells was not different from *3Myc-GFP* and *3FLAG-RBOHD* co-transfected cells (Fig. 3a). Enhancement of RBOHD activity by CRK2 was not dependent on Ca^{2+} influx as the elevated basal ROS production activity of RBOHD co-transfected with *CRK2-3Myc* ($ROS_{T=0}$ to $ROS_{T=30}$ in Fig. 3a) was also observed when using Ca^{2+}-free assay buffer (Figs. S3b and S3c). These results suggest that *CRK2-3Myc* enhanced the basal ROS-producing activity of 3FLAG-RBOHD in HEK293T cells uncoupling it from Ca^{2+} dependence.

The Arabidopsis genome encodes 10 *RBOHs* (Kaya et al., 2018). To test whether CRK2 specifically activates RBOHD, CRK2-3Myc was co-transfected with RBOHF and RBOHC into HEK293T cells. CRK2-3Myc enhanced basal ROS-producing activity of RBOHC and RBOHF in HEK293T cells similarly to RBOHD (Figs. S3d-S3g). However, while the basal ROS production activity ($ROS_{T=5}$) of RBOHD and F was elevated approximately 10fold, the basal activity of RBOHC was only elevated 3fold.

To investigate whether CRK2 and RBOHD interact *in planta,* we performed co-immunoprecipitation (Co-IP) assays using *rbohD* plants expressing *35S::CRK2-YFP* and *35S::FLAG-RBOHD*. CRK2-YFP was

immunoprecipitated using an anti-GFP antibody coupled to magnetic beads and co-purified RBOHD was detected using a RBOHD-specific antibody. RBOHD co-purified with CRK2 (Fig. 3b) and treatment of plants with flg22 did not alter the interaction of CRK2 with RBOHD (Fig. 3c). To analyze this interaction in more detail, we carried out *in vitro* interaction assays between the cytosolic region of CRK2 (Fig. 1a) and the cytosolic N-terminal and C-terminal regions of RBOHD (Fig. 3d). Recombinant RBOHD/N or RBOHD/C tagged with 6His and maltose-binding protein (MBP; 6His-MBP-RBOHD/N, 6His-MBP-RBOHD/C) or MBP were incubated with the cytosolic region of CRK2, which contains the kinase domain (CRK2cyto) tagged with 6His and glutathione S-transferase (GST; 6His-GST-CRK2cyto) and glutathione sepharose beads. GST pull-down assay showed that 6His-GST-CRK2cyto interacted *in vitro* with 6His-MBP-RBOHD/N but intriguingly also with 6His-MBP-RBOHD/C (Fig. 3e). In summary, our results suggest that CRK2 is capable of direct interaction with RBOHD. CRK2 and RBOHD form a complex which exists independent of flg22 perception *in planta*, in contrast to many other RLK-containing complexes which are formed in response to ligand-binding.

CRK2 phosphorylates RBOHD *in vitro*

The kinase activity of CRK2 was essential for the full flg22-triggered ROS burst *in planta* as well as for enhancing ROS production by RBOHD in HEK293T cells. Therefore, we tested whether CRK2 could phosphorylate RBOHD *in vitro*. Recombinant 6His-GST-CRK2cyto and 6His-MBP tagged RBOHD cytosolic regions (Figs. 1a and 3d) were produced in *E. coli* and affinity purified. The 6His-GST-CRK2cyto phosphorylated 6His-MBP-RBOHD/N but not MBP (Fig. 4a). Because of the similar molecular weight of 6His-GST-CRK2cyto (68.5 kDa) and 6His-MBP-RBOHD/C (78.4 kDa), RBOHD/C was divided into three overlapping fragments (C1, C2, and C3; Fig. 3d). The results showed that the C1 and C3 fragments of 6His-MBP-RBOHD were preferentially phosphorylated by 6His-GST-CRK2cyto while C2 displayed considerably weaker phosphorylation (Fig. 4b). Mass spectrometric analysis of in-gel trypsin- or Lys-C-digested peptides identified *in vitro* RBOHD phosphorylation sites targeted by CRK2cyto (Table S1). In the N-terminal region of RBOHD two sites targeted by CRK2 were identified (S8 and S39), while three sites (S611, S703, S862) were identified in the C-terminal region. Taken together our results show that the N- and C-terminal regions of RBOHD are phosphorylated by CRK2 *in vitro*.

CRK2 regulates RBOHD *via* phosphorylation of S703 and S862

Among the RBOHD phospho-sites targeted by CRK2 *in vitro*, phosphorylation of S8 and S39 has been previously described to be phosphorylated by SIK1 (Zhang et al., 2018) and BIK1 (Kadota et al., 2014, Li et al., 2014). S703 has been reported to be phosphorylated upon xylanase treatment but no responsible kinase was identified (Benschop et al., 2007) while phosphorylation of S611 and S862 has not been described so far. In order to test whether the identified phospho-sites in RBOHD were important for the regulation of RBOHD activity, the residues S8, S39, S611, S703, and S862 were substituted with alanine to make them non-phosphorylatable. Wild type RBOHD and phospho-site mutant constructs were transfected into HEK293T cells together with CRK2. Amino acid substitutions did not affect RBOHD protein levels (Fig. S4a and S4b).

Substitution of S8 or S39 in the N-terminal cytoplasmic region of RBOHD did not impact ROS-producing activity compared to the wild type protein when co-transfected with CRK2 (Fig. 5a). The 3FLAG-RBOHD^{S703A} and CRK2-3Myc co-transfected cells showed reduced basal ROS production as compared to 3FLAG-RBOHD and CRK2-3Myc, (Fig. 5b), suggesting that S703 could be a positive regulatory site for RBOHD activity. In contrast to 3FLAG-RBOHD^{S703A}, HEK293T cells expressing 3FLAG-RBOHD^{S862A} and CRK2-3Myc exhibited higher basal ROS production compared to 3FLAG-RBOHD and CRK2-3Myc (Fig. 5b), suggesting that S862 could act as a negative regulatory site. ROS production of 3FLAG-RBOHD^{S611A} co-transfected with CRK2-3Myc was similar to 3FLAG-RBOHD suggesting no regulatory role of this single site. Mutation of S703 or S862 of RBOHD did not impair Ca^{2+}-dependent activation of ROS production (Figs. S4c and S4d). Taken together, our results suggest that the phospho-sites in the C-terminal cytoplasmic region of RBOHD could be crucial for fine-tuning ROS production activity in HEK293T cells.

Phosphorylation of S703 of RBOHD modulates flg22-induced ROS production *in planta*

To investigate whether RBOHD phosphorylation sites targeted by CRK2 *in vitro* were also phosphorylated upon flg22-treatment *in planta*, we carried out targeted phosphoproteomic analyses of Col-0 plants treated with flg22 for 5 min. Phosphorylation of S8 was not significantly induced by flg22-treatment (Fig. 6a, S5a and S5b) while S39 phosphorylation was strongly enhanced (Fig. 6b and S5c). Phosphorylation of S611 and S862 could not be evaluated as trypsin or Lys-C digestion resulted in phospho-site-containing peptides of inappropriate length for LC-MS-based targeted analyses. However, phosphorylation of S703, which was targeted by CRK2 *in vitro* and mutation to alanine reduced ROS production in HEK293T cells, was significantly enhanced upon flg22 treatment (Fig. 6c and Fig. S5d). In agreement with previous studies, phosphorylation of S163, S343, and S347 in RBOHD (Fig. S5e-S5g), as well as dual phosphorylation of the TEY-motif in the MAPKs MPK3, MPK6 and MPK11 (Fig. S5h-S5j), were enhanced by flg22-treatment (Kadota, Shirasu et al., 2015). (Kadota et al., 2015)

To investigate whether phosphorylation of S703 in the C-terminal region of RBOHD also impacts RBOHD-dependent ROS production *in planta*, we generated transgenic plants expressing RBOHD or RBOHD^{S703A} under the control of the *RBOHD promoter* (*RBOHDpro::3FLAG-RBOHD*) in *rbohD* background. The phospho-site mutations did not alter growth or development compared to the 3FLAG-RBOHD expressing plants (Fig. S6a). Lines expressing similar amounts of 3FLAG-RBOHD or 3FLAG-RBOHD^{S703A} (Fig. S6b). Compared with 3FLAG-RBOHD expression lines, flg22-triggered ROS production in 3FLAG-RBOHD^{S703A} lines was significantly reduced (Figs. 6d and S6c). In summary, our results suggest that phosphorylation of S703 in the C-terminus of RBOHD is important for full flg22-triggered ROS production also *in planta*.

C-terminal phosphorylation sites are conserved in plant and animal NADPH oxidases

Since little is known about control of RBOH activity *via* its C-terminus we investigated whether regulation through S703 was unique to RBOHD or conserved also in other RBOHs. We constructed a phylogenetic tree of RBOHs from plant genomes representing major branches of the plant lineages (Fig. 7). Plant RBOHs

form a monophyletic group, which is separated from human NOX2 and NOX5. The phospho-sites in the C-terminal region displayed strong conservation throughout the plant RBOH clade. S703 was conserved in a monophyletic clade containing eight of the ten RBOHs from Arabidopsis but not in the clade containing RBOHH and RBOHJ (Fig. 7). The phospho-sites S611 as well as S862, which may be involved in negative regulation based on experiments in HEK293T cells (Fig. 5b), were strongly conserved in all plant RBOHs. The sequence motifs harboring S611 and S862 are intriguingly conserved even in human NOX2 and NOX5 (Fig. 7). The C-terminal region binds FAD and NADPH. Therefore it may underlie strong evolutionary constraints to conserve these binding properties. This may be also reflected in the strong conservation of C-terminal phospho-sites and their sequence context not only among plant NADPH oxidases but also animal NOX.

Discussion

CRKs are a large group of RLKs involved in biotic and abiotic stress signaling in Arabidopsis (Bourdais et al., 2015). We have previously shown that flg22-triggered extracellular ROS production is altered in several *crk* mutants (Bourdais et al., 2015). In particular CRK2, a member of the basal clade of CRKs (Vaattovaara et al., 2019), has been highlighted since *crk2* displays striking phenotypes (Bourdais et al., 2015) including reduced rosette size and reduced flg22-induced ROS production. Functional CRK2 restored the reduced rosette size (Fig. 1) as well as the MAMP-induced ROS burst (Fig. 2). In addition to their role in stress responses, extracellular ROS have also been implicated in leaf cell expansion (Schmidt et al., 2016), and the *rbohd rbohf* double mutant displays reduced rosette size (Torres et al., 2002). Overexpression of CRKs has been associated with increased SA accumulation (Acharya et al., 2007; Chen et al., 2004). However, since SA levels were unaltered in the loss-of-function mutant *crk2* (Fig. S1b), its smaller size may be a consequence of impaired ROS production (Fig. 2). This is supported by the observation that CRK2 enhanced the activity of RBOHD but also RBOHF in HEK293T cells (Fig. 3a and S3f). Alternatively, other substrates of CRK2 might be involved in the regulation of plant growth. In line with reduced MAMP- and DAMP-induced ROS production (Fig. 2a and 2b; Fig. S2c and S2d), *crk2* was more susceptible to the virulent bacterial pathogen *P*to DC3000 (Fig. 2c) suggesting that CRK2-mediated ROS production was essential to effectively counter pathogen infection. Also other flg22-induced defense responses were altered in *crk2* including reduced changes in cytosolic Ca^{2+} but enhanced callose deposition and MAPK activation (Fig. S2e-i). Ca^{2+} is important for the activation of RBOH but ROS also triggers Ca^{2+} fluxes in plants (Kimura et al., 2017). Thus, the diminished increase of cytosolic Ca^{2+} in *crk2* may be a consequence of the impaired flg22-induced ROS production. Also, callose deposition (Caillaud et al., 2014; Ellinger & Voigt, 2014) has been previously linked to ROS production (Couto & Zipfel, 2016) and CRK2 interacts with callose synthases and phosphorylates CALLOSE SYNTHASE 1 (CALS1) *in vitro* (Hunter et al., 2019). However, unlike in the response to flg22, salt-induced callose deposition is reduced in *crk2* (Hunter et al., 2019) suggesting that CRK2 might regulate different callose synthases in response to biotic and abiotic stimuli. Interestingly, CRK2 forms clusters at the plasma membrane in response to flg22-treatment and ROS is required for this process (Hunter et al., 2019). It is not clear how these clusters are integrated with the regulation of RBOHD activity but it might serve to connect RBOHD-dependent ROS production with callose deposition. Another important element in response to biotic and abiotic cues is the activation of MAPK cascades (Bigeard et al., 2015; Boudsocq et al., 2015) and earlier reports suggest a bifurcation to ROS burst and MAPK activation in defense signaling following MAMP-perception (Yeh et al., 2016; Zhang et al., 2007). CRK2 could be involved in balancing MAMP-induced ROS signaling pathways and MAPK signaling but the mechanisms are still unclear. Thus, CRK2 likely participates in the control of ROS production *via* interaction with RBOHD rather than MAMP-receptor complexes. Intriguingly, CRK2 existed in a pre-formed complex with RBOHD *in planta* independent of MAMP-treatment (Fig. 3c) while many other RLK protein complexes are formed upon signal perception.

Phosphorylation of the C-terminus is critical for the regulation of human NADPH oxidases. Phosphorylation of the NOX2 C-terminus by protein kinase C (PKC) enhances assembly of the multimeric NOX2 complex and its activity, whereas phosphorylation by *ataxia telangiectasia*-mutated (ATM) kinase inhibits NOX2 activity (Beaumel et al., 2017; Raad et al., 2009). NOX5 activity is regulated by Ca^{2+}-binding to EF-hands in the N-terminus (Banfi et al., 2004) but NOX5 is also activated by phosphorylation of the C-terminus by PKCα or calcium/calmodulin-dependent kinase II (CAMKII; Chen et al., 2014; Pandey et al., 2011). Although the C-terminal catalytic domain of RBOHs is highly conserved in plants and animal, the N-terminus has been considered as important for activation of the ROS-production activity and multiple phospho-sites (S8, S39, S133, S148, S163, S339, S334 and S347) have been reported. Intriguingly, CRK2cyto interacted with and phosphorylated the RBOHD C-terminal region at S611, S703 and S862 (Fig. 3e, 4b and Table S1). Phosphorylation of S703 upon xylanase treatment has been reported (Benschop et al., 2007) but not linked with other MAMPs or modulation of ROS production. Treatment of flg22 enhanced phosphorylation of S703 in Arabidopsis (Fig. 6c). Mutation S703A in RBOHD led to reduced CRK2-dependent RBOHD activity in HEK293T cells (Fig. 5b) and reduced flg22-induced ROS production in Arabidopsis (Fig. 6d). These results suggest that phosphorylation of the RBOHD C-terminus at S703 likely contributes to the regulation of MAMP-induced ROS production. Phosphorylation sites in the C-terminus were highly conserved among RBOHs (Fig. 7) suggesting that phosphorylation of the C-terminal region could be a general feature of plant NADPH oxidases. Remarkably, two putative RBOHD phospho-sites, S611 and S862, were identified even in the human NADPH oxidases NOX2 and NOX5 (Fig. 7). Substitution of RBOHD S862 to alanine resulted in enhanced ROS-producing activity in HEK293T cells. But substitution of RBOHD S611 to alanine, similarly to RBOHD S39A, did not alter ROS production in HEK293T cells (Fig. 5). RBOHD S39A also did not affect flg22-induced ROS production but phospho-mimic S39D enhanced the ROS production and phosphorylation of S39 is enhanced by MAMP treatment *in planta* (Kadota et al., 2014)(Fig. 6b, S5c). These results suggest the importance to determine the phosphorylation status of S611 and S862 *in planta*. RBOHD can also be regulated by cysteine S-nitrosylation in the C-terminus (Yun et al., 2011) but it is unclear how this modification is integrated with other regulatory mechanisms. Taken together, our results suggest that phosphorylation of the C-terminal region of plant NADPH oxidases is strongly conserved and important for controlling ROS production.

Several protein kinases phosphorylate RBOHD N-terminus and regulate the activity including RLCKs (Kadota et al., 2014; Li et al., 2014; Lin et al., 2015), MAP4Ks (Zhang et al., 2018), CPKs (Dubiella et al., 2013) and RLKs (Chen et al., 2017) but how is regulation by phosphorylation of the N- and C-terminal regions coordinated? BIK1 is a component involved in the activation of RBOHD by phosphorylation (Kadota et al., 2014; Li et al., 2014) and ROS production in *bik1* is reduced to a similar extent as in *crk2*. However, reduced flg22-induced ROS production in *crk2* was not due to lower *BIK1* transcript abundance (Fig. S7). BIK1 homologs, AvrPphB SUSCEPTIBLE1 (PBS1) and AvrPphB SUSCEPTIBLE1-LIKE (PBL) kinases, contribute to the regulation of RBOH activity and ROS production is progressively reduced in

329 double mutants with *bik1* (Lin et al., 2015; Zhang et al., 2018). CRK2 and BIK1 could synergistically
330 regulate ROS production but we were unable to obtain a double mutant between *bik1* and *crk2* (Table S2).
331 Therefore, we propose that at least one of these components is essentially required. BIK1 has previously
332 been shown to interact with other kinases including CRKs (Lee, 2017) but interaction with CRK2 has not
333 been investigated. BIK1 and CRK2 are likely highly coordinated in order to precisely control ROS
334 production in response to environmental stimuli (Fig. 8). Like CRKs, RBOHs are involved in diverse
335 processes in stress responses and also plant development and it is conceivable that different CRKs regulate
336 the diverse set of RBOH proteins in various cellular contexts potentially *via* phosphorylation of the C-
337 terminal region.

338 In summary, we propose that CRK2 is a central element in orchestrating the extracellular ROS burst and in
339 mediating the balance between different defense responses. The full complexity and integration of the
340 regulatory components controlling RBOH activity is still a topic of much speculation (Kimura et al. 2017).
341 The diversity of regulators converging at RBOHs reflects the prominent role of apoplastic ROS in signal
342 transduction while simultaneously strict control is required to circumnavigate oxidative damage. We suggest
343 that RBOHD is regulated by phosphorylation of the C-terminal region to complement regulatory
344 mechanisms targeting the N-terminus (Fig. 8). Based on the conservation of serine and threonine residues in
345 the C-terminus of NADPH oxidases we propose that this mode of regulation could be evolutionarily
346 conserved in plants and animals. In the future it will be interesting to investigate how CRK-mediated
347 phosphorylation of the RBOH C-terminus is integrated in the diverse processes which incorporate
348 extracellular ROS.

Materials and methods

Plant Material and growth condition

Arabidopsis thaliana plants used in this study include Col-0, *crk2* (Bourdais et al., 2015), *rbohD* (Torres et al., 2002), *fls2* (Zipfel et al., 2004), *bik1* (Veronese et al., 2006) and *35S::FLAG-RBOHD/rbohD* (Kadota et al., 2014). To generate *crk2/bik1* double mutant, *crk2* and *bik1* single mutant plants were crossed. F1, F2 and F3 progenies were analyzed by PCR. F2 and F3 seeds were obtained by self-pollination. Primers are listed in Table S3.

Seeds were sterilized by 70 % ethanol 2 % Triton X-100 for 5 min and washed 3 times with 99 % ethanol. Surface sterilized seeds were sown on 1x or ½ strength Murashige and Skoog (MS) medium containing 1 % sucrose and subsequently stratified for 2-4 days in the dark at 4 °C. Plants were grown in growth chambers (Panasonic, #MLR-352-PE) under 12 h light/12 h dark (22°C /18°C). After 10 days, seedlings were transferred to soil and grown in growth rooms under the following conditions: 12 h light/12 h dark (23 °C /19 °C), relative humidity 50-60 %, unless otherwise stated.

For SA measurements seedlings were grown in liquid culture as described (Denness et al., 2011) with minor modifications. 20 mg of seeds were sterilized by sequential incubation with 70 % ethanol and 50 % bleach on a rotating mixer for 10 min each and washed three times with sterile water. Seeds were then transferred into 250 mL Erlenmeyer flasks containing 125 mL ½ strength MS medium supplemented with 1 % sucrose. Seedlings were grown under long-day conditions (16 h light /8 h dark, 22 °C/18 °C) at 150 µmol m^{-2} s^{-1} photon flux density on an IKA KS501 flask shaker at a constant speed of 130 rotations per minute. Seedlings were collected after 6 days of growth.

Cell culture and Transfection

HEK293T cells (ATCC, #CRL-3216) were maintained at 37 °C in 5 % CO_2 in Dulbecco's Modified Eagle's Medium nutrient mixture Ham's F-12 (SIGMA, #D8062) supplemented with 10 % fetal bovine serum (Gibco, #26140-079). Cells were transfected with *pcDNA3.1* and *pEF1* vectors using GeneJuice transfection regent (Merck Millipore, #70967-3) according to the manufacturer's instructions.

Plasmid construction

CRK2 and *RBOHD* constructs for Arabidopsis were generated through MultiSite Gateway technology (Invitrogen). To generate pBm43GW-CRK2pro::CRK2-Venus (YFP)-3AT for *crk2* complementation lines, the coding region of *CRK2* or kinase-dead mutants (K353E or D450N) were recombined into pENTR/D-TOPO vector (Invitrogen). pDONRP4P1R/zeo-CRK2pro, pDONR/zeo-CRK2 (or pENTR/D-TOPO-CRK2 kinase-dead mutant) and p2R3a-VenusYFP-3AT were recombined with pBm43GW. To generate pHm43GW-pRBOHD::3FLAG-RBOHD-nosT, the coding region of 3FLAG-RBOHD was amplified by PCR from pcDNA3.1-3FLAG-RBOHD and cloned into pDONR/zeo vector (Invitrogen). The promoter region of *RBOHD* was amplified by PCR from pBin19g-pRBOHD::3FLAG-RBOHD and cloned into

pDONRP4P1R/zeo vector (Invitrogen). pDONRP4P1R/zeo-RBOHDpro, pDONR/zeo-3FLAG-RBOHD and p2R3a-nosT were recombined with pHm43GW. Single amino acid substitution mutants of *CRK2* and *RBOHD* were generated by point-mutant primers and the mega-primer PCR method. pBm43GW-CRK2pro::CRK2-YFP-3AT and pHm43GW-pRBOHD::3FLAG-RBOHD-nosT constructs were transformed into *crk2* and *rbohD* plants, respectively, by *Agrobacterium tumefaciens* strain GV3101 (pSoup)-mediated floral dipping (Clough & Bent, 1998). To generate *CRK2* over-expression lines for co-immunoprecipitation, pBm43GW-35S::CRK2-YFP-3AT were transformed into Col-0. p2R3a-Venus(YFP)-3AT, p2R3a-nosT, pBm43GW and pHm43GW (Siligato et al., 2016), pBin19g-pRBOHD::3FLAG-RBOHD (Kadota et al., 2014), pcDNA3.1-3FLAG-RBOHD (Kaya et al., 2018), pDONR/zeo-CRK2, pBm43GW-35S::CRK2-YFP-3AT and pDONRP4P1R/zeo-CRK2pro (Hunter et al., 2019) have been described previously.

6His-GST-CRK2cyto and 6His-MBP-RBOHD/C constructs for recombinant proteins were generated by using In-Fusion technology (Clontech). The coding regions of CRK2cyto (WT, K353E, and D450N), RBOHD/C (full-length, C1, C2, and C3) were amplified by PCR and cloned into pOPINK (Addgene, #41143) or pOPINM (Addgene, #26044) vectors. pOPINM-RBOHD/N was described previously (Kadota et al., 2014).

For HEK293T cell experiments, pEF1-MCS-3Myc [*Bam*HI-*Not*I-3Myc-stop fragment was inserted between *Kpn*I and *Xba*I sites of pEF1/myc-His B vector (Invitrogen)] was generated. To generate pEF1-CRK2 (WT or D450N)-3Myc, the codon optimized coding sequence of Kozak-CRK2 (WT or D450N) was cloned between *Bam*HI and *Not*I sites of pEF1-MCS-3Myc. To generate pcDNA3.1-3FLAG-RBOHD mutant constructs, the coding regions of RBOHD (S8A, S39A, S611A, S703A, or S862A) were cloned into *Bam*HI site of pcDNA3.1-3FLAG-MCS [Kozak-3FLAG-BamHI-EcoRV-stop fragment was inserted between *Nhe*I and *Kpn*I sites of pcDNA3.1(-) vector (Invitrogen)]. Amino acid substituted mutants of CRK2 and RBOHD were generated by point-mutant primers and the mega-primer PCR method. pEF1-3Myc-GFP (Kawarazaki, Kimura et al., 2013), pcDNA3.1-3FLAG-RBOHD, pcDNA3.1-3FLAG-RBOHC, pcDNA3.1-3FLAG-RBOHF and pcDNA3.1-3FLAG-MCS were described previously (Kaya et al., 2018). Primer sequences are listed in the Table S3.

Subcellular protein localization

Fluorescent images were obtained using a Leica TCS SP5 II HCS confocal microscope. For investigation of CRK2-YFP localization, 514 nm excitation and 525-590 nm detection range were used.

ROS measurements

Leaf discs were collected using a cork borer from 4-week-old *Arabidopsis* plants and floated overnight in sterile distilled water in 96 well plates under continuous light at room temperature. On the following day, water was replaced with assay buffer containing 34 mg/L luminol sodium salt (Sigma, #A4685), 20 mg/L horse radish peroxidase (Fujifilm Wako, #169-10791), 200 nM flg22 (GenScript), 200 µg/mL Chitin (Sigma,

#C9752) or 1 μM AtPep1 (ATKVKAKQRGKEKVSSGRPGQHN: synthesized by Synpeptide, China). Luminescence was measured for 1 sec every 1 min at room temperature using GloMax-Multi+Detection System (Promega). ROS production was expressed in relative luminescence units (RLU).

The ROS producing activity of RBOHs in HEK293T cells was measured as described previously (Kimura et al., 2012). Two days after transfection, medium was removed and cells were gently washed with 1xHBSS (GIBCO, #14025-092 or #14175-095). Measurements were started after addition of the assay buffer containing 250 μM lunimol sodium salt and 66.7 mg/L horse radish peroxidase. After 30 min measurement, 1μM ionomycin (Calbiochem, #407952) was added. Chemiluminescence was measured for 1 sec every 1 min at 37 °C using GloMax-Multi+Detection System. ROS production was expressed in relative luminescence units (RLU). Expressed proteins were detected by immunoblotting with anti-FLAG (Sigma, #F1804), anti-cMyc (Fujifilm Wako, #017-2187), anti-β-actin (Sigma, #A5316) and IRDye800CW anti-mouse IgG (LI-COR, #926-32210) antibodies.

Bacterial growth assay

To quantify bacterial growth on 4-week-old plants infected with the virulent *Pto*DC3000 (Whalen et al., 1991), growth curve assays were performed as described previously (Wrzaczek et al., 2007).

Ca^{2+} imaging

Calcium imaging with YCNano-65 expressing plants was performed as described previously (Choi et al., 2014, Lenglet et al., 2017, Toyota et al., 2018). In brief, YCNano-65 was visualized by a fluorescence stereo microscope (Nikon) with a 1× objective lens (Nikon), image splitting optics (Hamamatsu Photonics) and a sCMOS camera (Hamamatsu Photonics). To excite YCNano-65, a mercury lamp (Nikon), a 436/20 nm excitation filter (Chroma) and a 455 nm dichroic mirror (Chroma) were used. The fluorescent signal from YCNano-65 was separated by a 515 nm dichroic mirror (Chroma) equipped in the image splitting optics. The resultant CFP and YFP (FRET) signals passed independently through a 480/40 nm and 535/30 nm emission filters, respectively (Chroma). A pair of the CFP and FRET images was simultaneously acquired every 4 s with the sCMOS camera using NIS-Elements imaging software (Nikon). Approximately 2 μL of 1 μM flg22 was applied to the adaxial surface of cotyledons in 7-day-old seedlings, in which a region of interest (ROI) was placed to analyze both CFP and FRET signals. The FRET/CFP ratio was calculated by the 6D imaging plug-in modules (Nikon).

MAPK assay

MAPK assays were performed as previously described (Yadeta et al., 2017). In brief, 4-week-old Arabidopsis plants were sprayed with 10 μM flg22 with 0.025 % Silwett L-77. Leaf samples were ground in liquid nitrogen and sand. Extraction buffer [50 mM HEPES (pH7.4), 50 mM NaCl, 10 mM EDTA, 0.2 % Triron X-100, 1 % Protease inhibitor cocktail (SIGMA, #P9599), 1 % Halt phosphatase inhibitor cocktail (Thermo scientific, #78428)] was added (2 mL/g plant powder). Samples were incubated at 4 °C for 30 min

and centrifuged at 12,000 x g, 4 °C for 10 min. The supernatant was used for immunoblotting with anti-Phospho-p44/42 MAPK (Cell Signaling Technology, #4370) and IRDye800CW anti-rabbit IgG (LI-COR, #926-32211) antibodies.

Callose Staining

Callose staining was performed as described previously (Hunter et al., 2019).

qRT-PCR

Col-0, *crk2* and *fls2* seedlings were grown on MS 1 % sucrose agar plate for 5 days and were transferred into MS 1 % sucrose liquid media and grown for 5 days. Plants were incubated with 1 µM flg22 for 30 min, 1 h and 3 h, respectively. Plants were ground in liquid nitrogen and total RNA was extracted using the GeneJET Plant RNA purification Kit (Thermo scientific, #K0802). Total RNA was treated with DNase I (Thermo scientific, #EN0525) and cDNA was synthesized with Maxima H Minus Reverse Transcriptase (Thermo scientific, #EP0751). qPCR analysis was performed with CFX real-time PCR (BioRad, Hercules, CA, US) using 5× HOT FIREPol EvaGreen qPCR Mix Plus ROX (Soils Biodyne). *SAND*, *TIP41* and *YLS8* were used as reference genes for normalization. Relative expression was calculated with qBase+ (Biogazelle; https://www.qbaseplus.com/). Primers are listed in Table S3.

Phytohormone analysis

SA was analyzed from liquid-cultured seedlings as described previously (Forcat, Bennett et al., 2008) with minor modifications. Seedlings were flash-frozen in liquid nitrogen and freeze-dried for 24 h. About 6 mg aliquots of freeze-dried material were homogenized by shaking with 5 mm stainless steel beads in a Qiagen Tissue Lyser II for 2 min at 25 Hz. Shaking was repeated after addition of 400 µL extraction buffer (10 % methanol, 1 % acetic acid) with internal standard (28 ng Salicylic-d_4 Acid; CDN Isotopes, Pointe-Claire, Canada). Samples were then incubated on ice for 30 min and centrifuged for 10 min at 16,000 x g and 4 °C. Supernatants were transferred into fresh 2 mL tubes and pellets were re-extracted with 400 µL extraction buffer without internal standards. Supernatants were combined and centrifuged 3 times to remove all debris before LC-MS/MS analysis.

The chromatographic separation was carried out using an Acquity UHPLC Thermo system (Waters, Milford, U.S.) equipped with a Waters Cortecs C18 column (2.7 µm, 2.1 x 100 mm). The solvent gradient (acetonitrile (ACN) / water with 0.1 % formic acid each) was adapted to a total run time of 7 min: 0-4 min 20 % to 95 % ACN, 4-5 min 95 % ACN, 5-7 min 95 % to 20 % ACN; flow rate 0.4 mL / min. For hormone identification and quantification, a tandem mass spectrometric system Xevo TQ-XS, triple quadrupole mass analyser (QqQ) with a ZSpray ESI function (Waters, Milford, U.S.) was used. Mass transitions were: SA 137 > 93, D_4-SA 141 > 97.

Protein extraction and Co-immunoprecipitation

Co-immunoprecipitation was performed as described previously (Kadota et al., 2016). Homozygous *35S::FLAG-RBOHD/rbohD* was crossed with homozygous *35S::CRK2-YFP/Col-0* or *35S::YFP-6Myc/Col-0*. *35S::FLAG-RBOHD/35S::CRK2-YFP/rbohD* F3 plants were selected by kanamycin resistance (homozygous FLAG-RBOHD insertion) and PCR (homozygous *rbohD* T-DNA insertion). F1 and F3 plants were grown on MS 1 % sucrose agar plate for 7 days and were transferred into MS 1 % sucrose liquid media and grown for 8-10 days. F3 plants were incubated in water or 1 µM flg22 for 10 min or 30 min after vacuum application for 2 min. Plants were ground in liquid nitrogen and sand. Extraction buffer [50 mM Tris-HCl (pH 7.5), 150 mM NaCl, 10 % Glycerol, 5 mM DTT, 1 % Protease inhibitor cocktail (SIGMA, P9599), 2 % IGEPAL CA630, 1 mM $Na_2MoO_42H_2O$, 2.5 mM NaF, 1.5 mM Activated sodium orthovanadate, 1 mM PMSF] was added at 1.5 - 2 mL/g fresh weight. Samples were incubated at 4 °C for 1 h and centrifuged at 15,000 x g, 4 °C for 20 min. Supernatants were adjusted to 5 mg/mL protein concentration and incubated for 1 h at 4 °C with 100 µL of anti-GFP magnetic beads (Miltenyi Biotec, #130-091-125). Bound proteins were analyzed by immunoblotting with anti-GFP (Invitrogen, #A11122), anti-RBOHD (Agrisera, #AS15-2962), and IRDye800CW anti-rabbit IgG (LI-COR, #926-32211) antibodies.

To detect 3FLAG-RBOHD, total protein was extracted from *RBOHDpro::3FLAG-RBOHD (WT or S703A)/rbohD* T3 homozygous plants with the same extraction buffer and analyzed by immunoblotting with anti-FLAG (Sigma, #F1804 and IRDye800CW anti-mouse IgG (LI-COR, #926-32210) antibodies.

Protein purification from *E.coli*

Cytosolic regions of CRK2 were expressed in *Escherichia coli* Lemo21. Cytosolic regions of RBOHD and Maltose binding protein (MBP) were expressed in *Escherichia coli* BL21. Glutathione S transferase (GST)-tagged recombinant proteins were purified using glutathione sepharose 4B (GE Healthcare, #17-0756-01) according to manufacturer's instructions. MBP-tagged proteins were purified using amylose resin (New England Biolabs, #E8021S) according to manufacturer's instructions.

***In vitro* pull down**

6His-GST-CRK2cyto, 6His-MBP-RBOHD/N, 6His-MBP-RBOHD/C and MBP were incubated with glutathione Sepharose 4B in the pull down buffer (20 mM HEPES, 50 mM KCl, 5 mM $MaCl_2$, 1 % Tween20, 1 mM DTT and 100 µM PMSF) at 4 °C for 1 h. The glutathione sepharose 4B was washed four times with the pull down buffer and eluted with 10 mM reduced gluthatione. The mixture was analyzed by immunoblotting anti-6xHis (Invitrogen, #MA1-135), anti-MBP (Santa Cruz Biotechnology, #sc-13564) and IRDy800CW anti-mouse IgG antibodies.

***In vitro* kinase assay**

Purified recombinant proteins were incubated with [γ-^{32}P] for 30 min at room temperature in the kinase assay buffer [50 mM HEPES (pH7.4), 1 mM DTT, 10 mM $MgCl_2$, 0.6 mM unlabeled ATP]. The mixture was

subsequently separated by SDS-PAGE and autoradiography was detected by FLA-5100 image analyzer (Fujifilm, Japan). For identification of *in vitro* phosphorylation sites by LC-ESI-MS/MS, 1.5 mM unlabeled ATP was used in the kinase buffer. The proteins were separated by SDS-PAGE, followed by CBB staining and were digested by trypsin (Thermo scientific, #90057) or Lys-C (Thermo scientific, #90051).

Identification of *in vitro* phosphorylation sites of RBOHD by LC-ESI-MS/MS

Trypsin or Lys-C digested protein samples were analyzed by a Q Exactive mass spectrometer (Thermo Fisher Scientific, Bremen, Germany) connected to Easy NanoLC 1000 (Thermo Fisher Scientific). Peptides were first loaded on a trapping column and subsequently separated inline on a 15 cm C18 column (75 µm x 15 cm, ReproSil-Pur 5 µm 200 Å C18-AQ, Dr. Maisch HPLC GmbH, Ammerbuch-Entringen, Germany). The mobile phase consisted of water with 0.1 % formic acid (solvent A) or acetonitrile/water [80:20 (v/v)] with 0.1 % formic acid (solvent B). A linear 10 min gradient from 8 % to 42 % B was used to elute peptides.

MS data was acquired automatically by using Thermo Xcalibur 3.1 software (Thermo Fisher Scientific). An information dependent acquisition method consisted of an Orbitrap MS survey scan of mass range 300-2000 m/z followed by HCD fragmentation for 10 most intense peptide ions. Raw data was searched for protein identification by Proteome Discoverer (version 2.2) connected to in-house Mascot (v. 2.6.1) server. Phosphorylation site locations were validated using phosphoRS algorithm. A SwissProt database with a taxonomy filter *Arabidopsis thaliana* was used. Two missed cleavages were allowed. Peptide mass tolerance ± 10 ppm and fragment mass tolerance ± 0.02 Da were used. Carbamidomethyl (C) was set as a fixed modification and methionine oxidation, acetylation of protein N-terminus, phosphorylation of Ser and Thr were included as variable modifications. Only peptides with FDR 0.01 were used.

Targeted (phospho) peptide analysis

Plant treatment and phosphopeptide enrichment. Arabidopsis seeds were sterilized by incubating with 1.5 % NaClO 0.02 % Triton X-100 solution for 5 min and vernalized at 4 °C for 2 days. Sterilized seeds were germinated and grown in liquid culture on 6 well plates (30 seeds/well) in MGRL medium with 0.1 % (w/v) sucrose (2 mL/well; Fujiwara et al., 1992) at 23 °C under continuous light (100 µmol m^{-2} s^{-1}) in a Percival growth chamber. Plates with 11-day-old seedlings were transferred from the growth chamber to a workbench and kept o/n for acclimatization before treatments. Seedlings were treated with either 1 µM flg22 or sterile water for 5 min after which seedlings were immediately collected and flash-frozen in liquid nitrogen and stored at -80 °C. Frozen seedlings were disrupted using a Retsch mill (5 min, 30 Hz), and 500 µL urea extraction buffer [8M urea in 100mM Tris, pH 8.5, 20 µL/mL Phosphatase Inhibitor Cocktail 3 (Sigma, P0044), 20 µL/mL Phosphatase Inhibitor Cocktail 2 (Sigma, P5726), 5 mM DTT] was added to the disrupted frozen powders, mixed briefly and incubated at RT for 30 min. After centrifugation at 15,000 x g for 10 min, supernatants were transferred to fresh tubes. Protein concentrations were determined using Pierce 660 nm protein assay (Thermo Scientific). Extracts with 500 µg of protein were alkylated with 14 mM chloroacetamide (CAA) at RT for 30 min in the dark, CAA was quenched by addition of 1/200 sample

volume 1M DTT. Samples were diluted 1:8 with 0.1 M Tris, pH 8.5, 1 mM $CaCl_2$ and were digested o/n at RT either with 5 µg trypsin or 5 µg Lys-C. Digestion reaction was terminated by addition of TFA (0.1 % final concentration), and peptides were desalted using C18 SepPaks [1cc cartridge, 100 mg (WAT023590)]. In brief, SepPaks were conditioned using methanol (1 mL), buffer B (80 % acetonitrile, 0.1 % TFA; 1 mL) and buffer A (0.1 % TFA; 2 mL). Samples were loaded by gravity flow, washed with buffer A (1 x 1 mL, 1 x 2 mL) and eluted with buffer B (2 x 400 µL). 40 µL of eluates were kept separately to measure non-phosphopeptides and the rest were used for further phosphopeptide enrichment. Phosphopeptide enrichment was performed by hydroxy acid-modified metal-oxide chromatography (HAMMOC) using titania as described previously with minor modifications (Nakagami, 2014; Sugiyama et al., 2007).

LC-MS/MS data acquisition. Samples were analyzed using an EASY-nLC 1200 (Thermo Fisher) coupled to a Q Exactive Plus mass spectrometer (Thermo Fisher). Peptides were separated on 16 cm frit-less silica emitters (New Objective, 0.75 µm inner diameter), packed in-house with reversed-phase ReproSil-Pur C18 AQ 1.9 µm resin (Dr. Maisch). Peptides were loaded on the column and eluted for 115 min using a segmented linear gradient of 5 % to 95 % solvent B (0 min, 5 % B; 0-5 min, 5 % B; 5-65 min, 20 % B; 65-90 min, 35 % B; 90-100 min, 55 % B; 100-105 min, 95 % B; 105-115 min, 95 % B) [solvent A (0 % ACN, 0.1 % FA); solvent B (80 % ACN, 0.1 % FA)] at a flow rate of 300 nL/min. Mass spectra were acquired using a targeted (parallel reaction monitoring, PRM) approach. The acquisition method consisted of a full scan method combined with a non-scheduled PRM method. The 16 targeted precursor ions were selected based on the results of a DDA peptide search of phospho-enriched samples in Skyline (MacLean, Tomazela et al., 2010) (Version 4.2.0.x, https://skyline.ms). MS spectra were acquired in the Orbitrap analyzer with a mass range of 300–1750 m/z at a resolution of 70,000 FWHM and a target value of 3×10^6 ions, followed by MS/MS acquisition for the 16 targeted precursors. Precursors were selected with an isolation window of 2.0 m/z. HCD fragmentation was performed at a normalized collision energy of 27. MS/MS spectra were acquired with a target value of $2x10^5$ ions at a resolution of 17,500 FWHM, a maximum injection time of 120 ms and a fixed first mass of m/z 100.

MS data analysis. Raw data from PRM acquisition were processed using MaxQuant software (version 1.5.7.4, http://www.maxquant.org/; Cox & Mann, 2008). MS/MS spectra were searched by the Andromeda search engine against a combined database containing the sequences from *Arabidopsis thaliana* (TAIR10_pep_20101214; ftp://ftp.arabidopsis.org/home/tair/Proteins/TAIR10_protein_lists/) and sequences of 248 common contaminant proteins and decoy sequences. Trypsin specificity was required and a maximum of two missed cleavages allowed. Minimal peptide length was set to seven amino acids. Carbamidomethylation of cysteine residues was set as fixed, phosphorylation of serine, threonine and tyrosine, oxidation of methionine and protein N-terminal acetylation as variable modifications. The match between runs option was disabled. Peptide-spectrum-matches and proteins were retained if they were below a false discovery rate of 1 % in both cases. The “msms.txt” output from MaxQuant was further analyzed

using Skyline in PRM mode. Trypsin specificity was required and a maximum of two missed cleavages allowed. Minimal and maximum peptide lengths were set to 7 and 25 amino acids, respectively. Carbamidomethylation of cysteine, phosphorylation of serine, threonine and tyrosine, oxidation of methionine, and protein N-terminal acetylation were set as modifications. Results were filtered for precursor charges of 2 and 3, and b- and y-ions with ion charges of +1 and +2. Product ions were set to "from ion 1 to last ion". All chromatograms were inspected manually and peak integration was corrected for best representation of MS2 signals. Peak area data was exported and further processed. The Skyline documents containing the data for the targeted phophoproteomics experiments have been uploaded to Panorama Public and can be obtained from https://panoramaweb.org/RBOHDphosphorylation.url. Raw data have been deposited to the ProteomeXchange Consortium via the Panorama partner repository with the dataset identifier PXD013525 (http://proteomecentral.proteomexchange.org/cgi/GetDataset?ID=PXD013525).

Phylogenetic analysis

Sequences for plant *RBOH* genes were extracted from public genome databases and manually curated. The phylogenetic maximum likelihood tree was inferred from a PAGAN (Löytynoja et al., 2012) alignment using FASTTREE (Price et al., 2010), 1000 bootstrap replicates were calculated using RAxML (Stamatakis, 2014). The sequence alignment of plant RBOHs, human NOX2 and NOX5ß can be viewed on the Wasabi (Veidenberg et al., 2016) webserver (http://was.bi?id=JauZ6q). Sequence motifs were analyzed using the MEME suite (Bailey et al., 2009).

Statistical analysis

Statistical analyses were performed with JMP Pro13 (SAS, https://www.jmp.com/).

Data availability

Phylogenetic tree of human and plant NADPH oxidases with bootstrap information for 1000 replicates and corresponding sequence alignment has been deposited on Wasabi (http://wasabiapp.org). Data for the targeted phophoproteomics experiments has been uploaded to Panorama Public (https://panoramaweb.org/RBOHDphosphorylation.url). Raw data have been deposited to the ProteomeXchange Consortium via the Panorama partner repository with the dataset identifier PXD013525 (http://proteomecentral.proteomexchange.org/cgi/GetDataset?ID=PXD013525). Materials used in the experimental work are available from the authors upon request.

615 **Author contributions**

616 SK, KH, HN and MW conceived and designed the project. SK, KH, LV, CT, AV, AR, LM, MWi, MT, and
617 MWr carried out experiments. SK, KH, LV, AV, AR, TH, MT, and MWr analyzed the data. AH, SCS and
618 HN designed and performed targeted MS analysis and analyzed the data. SK and MWr wrote the manuscript.
619 All authors read and contributed to the final manuscript.

620 **Acknowledgments**

621 The authors would like to thank Dr. Julia Krasensky-Wrzaczek and Dr. Alexey Shapiguzov (University of
622 Helsinki, Finland) for critical comments on the manuscript. We thank Tuomas Puukko, Nghia Le Tri, Simon
623 Schmitz, Denis Owczarek, Jan-Niklas Weber (University of Helsinki, Finland) and Jiaqi Wang (Saitama
624 University, Japan) for technical assistance, Dr. Riccardo Siligato for the Gateway Multisite vector system.
625 LV and TH thank Trude Johansen for technical assistance in LC-MS/MS based hormone analysis. We thank
626 Dr. Yasuhiro Kadota (RIKEN Yokohama, Japan) and Prof. Cyril Zipfel (University of Zurich, Switzerland)
627 for *35S::FLAG-RBOHD/rbohD* seeds and pOPINM-RBOHD/N and pBin19g-pRBOHD::3FLAG-RBOHD
628 plasmids. We thank Prof. Simon Gilroy (University of Wisconsin, USA) for *YCNano65* seeds. The
629 pcDNA3.1-3FLAG-RBOHD and pcDNA3.1-3FLAG-MCS plasmids were provided by Prof. Kazuyuki
630 Kuchitsu (Tokyo University of Science, Japan). Microscopy imaging was performed at the Light Microscopy
631 Unit, Institute of Biotechnology, University of Helsinki. Mass spectrometry analyses were performed at the
632 Turku Proteomics Facility, supported by Biocenter Finland. This work was supported by the Academy of
633 Finland (grant numbers #275632, #283139, and #312498 to MW), the University of Helsinki (Three-year
634 fund allocation to MW), the Finnish Cultural Foundation (grant numbers 00170046 and 00181379 to LV),
635 and KAKENHI (17H05007, 18H04775, and 18H05491 to MT), the Max-Planck-Gesellschaft (to HN). KH,
636 SK, AV and MW are members of the Centre of Excellence in the Molecular Biology of Primary Producers
637 (2014-2019) funded by the Academy of Finland (grant numbers #271832 and #307335).

638

References

Acharya BR, Raina S, Maqbool SB, Jagadeeswaran G, Mosher SL, Appel HM, Schultz JC, Klessig DF, Raina R (2007) Overexpression of CRK13, an Arabidopsis cysteine-rich receptor-like kinase, results in enhanced resistance to *Pseudomonas syringae*. *Plant J* 50: 488-499

Bailey TL, Boden M, Buske FA, Frith M, Grant CE, Clementi L, Ren J, Li WW, Noble WS (2009) MEME SUITE: tools for motif discovery and searching. *Nucleic Acids Res* 37: W202-8

Banfi B, Tirone F, Durussel I, Knisz J, Moskwa P, Molnar GZ, Krause KH, Cox JA (2004) Mechanism of Ca^{2+} activation of the NADPH oxidase 5 (NOX5). *J Biol Chem* 279: 18583-18591

Beaumel S, Picciocchi A, Debeurme F, Vives C, Hesse AM, Ferro M, Grunwald D, Stieglitz H, Thepchatri P, Smith SME, Fieschi F, Stasia MJ (2017) Down-regulation of NOX2 activity in phagocytes mediated by ATM-kinase dependent phosphorylation. *Free Radic Biol Med* 113: 1-15

Benschop JJ, Mohammed S, O'Flaherty M, Heck AJ, Slijper M, Menke FL (2007) Quantitative phosphoproteomics of early elicitor signaling in *Arabidopsis*. *Mol Cell Proteomics* 6: 1198-1214

Bigeard J, Colcombet J, Hirt H (2015) Signaling mechanisms in pattern-triggered immunity (PTI). *Mol Plant* 8: 521-539

Boudsocq M, Danquah A, de Zelicourt A, Hirt H, Colcombet J (2015) Plant MAPK cascades: Just rapid signaling modules? *Plant Signal Behav* 10: e1062197

Bourdais G, Burdiak P, Gauthier A, Nitsch L, Salojärvi J, Rayapuram C, Idänheimo N, Hunter K, Kimura S, Merilo E, Vaattovaara A, Oracz K, Kaufholdt D, Pallon A, Anggoro DT, Glów D, Lowe J, Zhou J, Mohammadi O, Puukko T et al. (2015) Large-scale phenomics identifies primary and fine-tuning roles for CRKs in responses related to oxidative stress. *PLOS Genetics* 11: e1005373

Caillaud MC, Wirthmueller L, Sklenar J, Findlay K, Piquerez SJ, Jones AM, Robatzek S, Jones JD, Faulkner C (2014) The plasmodesmal protein PDLP1 localises to haustoria-associated membranes during downy mildew infection and regulates callose deposition. *PLoS Pathog* 10: e1004496

Chen D, Cao Y, Li H, Kim D, Ahsan N, Thelen J, Stacey G (2017) Extracellular ATP elicits DORN1-mediated RBOHD phosphorylation to regulate stomatal aperture. *Nat Commun* 8: 2265

Chen F, Yu Y, Haigh S, Johnson J, Lucas R, Stepp DW, Fulton DJ (2014) Regulation of NADPH oxidase 5 by protein kinase C isoforms. *PLoS One* 9: e88405

Chen K, Fan B, Du L, Chen Z (2004) Activation of hypersensitive cell death by pathogen-induced receptor-like protein kinases from *Arabidopsis*. *Plant Mol Biol* 56: 271-283

Chern M, Xu Q, Bart RS, Bai W, Ruan D, Sze-To WH, Canlas PE, Jain R, Chen X, Ronald PC (2016) A genetic screen identifies a requirement for cysteine-rich-receptor-like kinases in rice NH1 (OsNPR1)-mediated immunity. *PLoS Genet* 12: e1006049

Choi WG, Toyota M, Kim SH, Hilleary R, Gilroy S (2014) Salt stress-induced Ca^{2+} waves are associated with rapid, long-distance root-to-shoot signaling in plants. *Proc Natl Acad Sci USA* 111: 6497-6502

Clough SJ, Bent AF (1998) Floral dip: a simplified method for *Agrobacterium*-mediated transformation of *Arabidopsis thaliana*. *Plant J* 16: 735-743

Couto D, Zipfel C (2016) Regulation of pattern recognition receptor signalling in plants. *Nat Rev Immunol* 16: 537-552

Cox J, Mann M (2008) MaxQuant enables high peptide identification rates, individualized p.p.b.-range mass accuracies and proteome-wide protein quantification. *Nat Biotechnol* 26: 1367-1372

Denness L, McKenna JF, Segonzac C, Wormit A, Madhou P, Bennett M, Mansfield J, Zipfel C, Hamann T (2011) Cell wall damage-induced lignin biosynthesis is regulated by a reactive oxygen species- and jasmonic acid-dependent process in Arabidopsis. *Plant Physiol* 156: 1364-1374

Dubiella U, Seybold H, Durian G, Komander E, Lassig R, Witte CP, Schulze WX, Romeis T (2013) Calcium-dependent protein kinase/NADPH oxidase activation circuit is required for rapid defense signal propagation. *Proc Natl Acad Sci USA* 110: 8744-8749

686 Ellinger D, Voigt CA (2014) Callose biosynthesis in Arabidopsis with a focus on pathogen response: what
687 we have learned within the last decade. *Ann Bot* 114: 1349-1358
688 Forcat S, Bennett MH, Mansfield JW, Grant MR (2008) A rapid and robust method for simultaneously
689 measuring changes in the phytohormones ABA, JA and SA in plants following biotic and abiotic stress.
690 *Plant Methods* 4: 16
691 Fujiwara T, Hirai MY, Chino M, Komeda Y, Naito S (1992) Effects of sulfur nutrition on expression of the
692 soybean seed storage protein genes in transgenic petunia. *Plant Physiol* 99: 263-268
693 Han JP, Koster P, Drerup MM, Scholz M, Li S, Edel KH, Hashimoto K, Kuchitsu K, Hippler M, Kudla J
694 (2019) Fine-tuning of RBOHF activity is achieved by differential phosphorylation and Ca^{2+} binding. *New*
695 *Phytol* 221: 1935-1949
696 Hunter K, Kimura S, Rokka A, Tran HC, Toyota M, Kukkonen JP, Wrzaczek M (2019) CRK2 enhances salt
697 tolerance by regulating callose deposition in connection with PLDalpha1. *Plant Physiol*
698 Idänheimo N, Gauthier A, Salojärvi J, Siligato R, Brosché M, Kollist H, Mähönen AP, Kangasjärvi J,
699 Wrzaczek M (2014) The *Arabidopsis thaliana* cysteine-rich receptor-like kinases CRK6 and CRK7 protect
700 against apoplastic oxidative stress. *Biochem Biophys Res Commun* 445: 457-462
701 Jagnandan D, Church JE, Banfi B, Stuehr DJ, Marrero MB, Fulton DJ (2007) Novel mechanism of activation
702 of NADPH oxidase 5. Calcium sensitization via phosphorylation. *J Biol Chem* 282: 6494-6507
703 Jiménez-Quesada MJ, Traverso JA, Alché Jde D (2016) NADPH oxidase-dependent superoxide production
704 in plant reproductive tissues. *Front Plant Sci* 7: 359
705 Kadota Y, Macho AP, Zipfel C (2016) Immunoprecipitation of plasma membrane receptor-like kinases for
706 identification of phosphorylation sites and associated proteins. *Methods Mol Biol* 1363: 133-144
707 Kadota Y, Shirasu K, Zipfel C (2015) Regulation of the NADPH Oxidase RBOHD During Plant Immunity.
708 *Plant Cell Physiol* 56: 1472-80
709 Kadota Y, Sklenar J, Derbyshire P, Stransfeld L, Asai S, Ntoukakis V, Jones JD, Shirasu K, Menke F, Jones
710 A, Zipfel C (2014) Direct regulation of the NADPH oxidase RBOHD by the PRR-associated kinase BIK1
711 during plant immunity. *Mol Cell* 54: 43-55
712 Kawarazaki T, Kimura S, Iizuka A, Hanamata S, Nibori H, Michikawa M, Imai A, Abe M, Kaya H,
713 Kuchitsu K (2013) A low temperature-inducible protein AtSRC2 enhances the ROS-producing activity of
714 NADPH oxidase AtRbohF. *Biochim Biophys Acta* 1833: 2775-2780
715 Kaya H, Takeda S, Kobayashi MJ, Kimura S, Iizuka A, Imai A, Hishinuma H, Kawarazaki T, Mori K,
716 Yamamoto Y, Murakami Y, Nakauchi A, Abe M, Kuchitsu K (2018) Comparative analysis of the reactive
717 oxygen species-producing enzymatic activity of Arabidopsis NADPH oxidases. *Plant J*
718 Kimura S, Kaya H, Kawarazaki T, Hiraoka G, Senzaki E, Michikawa M, Kuchitsu K (2012) Protein
719 phosphorylation is a prerequisite for the Ca^{2+}-dependent activation of *Arabidopsis* NADPH oxidases and
720 may function as a trigger for the positive feedback regulation of Ca^{2+} and reactive oxygen species. *Biochim*
721 *Biophys Acta* 1823: 398-405
722 Kimura S, Waszczak C, Hunter K, Wrzaczek M (2017) Bound by fate: The role of reactive oxygen species in
723 receptor-like kinase signaling. *Plant Cell* 29: 638-654
724 Lee DSK, Young Cheon; Kwon, Sun Jae; Ryu, Choong-Min; Park, Ohkmae K. (2017) The Arabidopsis
725 cysteine-rich receptor-like kinase CRK36 regulates immnity through interaction with the cytoplasmic kinase
726 BIK1. *Frontiers in Plant Science* 8: 1856
727 Lee Y, Rubio MC, Alassimone J, Geldner N (2013) A mechanism for localized lignin deposition in the
728 endodermis. *Cell* 153: 402-412
729 Lee Y, Yoon TH, Lee J, Jeon SY, Lee JH, Lee MK, Chen H, Yun J, Oh SY, Wen X, Cho HK, Mang H,
730 Kwak JM (2018) A lignin molecular brace controls precision processing of cell walls critical for surface
731 integrity in *Arabidopsis*. *Cell* 173: 1468-1480

Lenglet A, Jaslan D, Toyota M, Mueller M, Muller T, Schonknecht G, Marten I, Gilroy S, Hedrich R, Farmer EE (2017) Control of basal jasmonate signalling and defence through modulation of intracellular cation flux capacity. *New Phytol* 216: 1161-1169

Li L, Li M, Yu L, Zhou Z, Liang X, Liu Z, Cai G, Gao L, Zhang X, Wang Y, Chen S, Zhou JM (2014) The FLS2-associated kinase BIK1 directly phosphorylates the NADPH oxidase RbohD to control plant immunity. *Cell Host Microbe* 15: 329-338

Lin ZJ, Liebrand TW, Yadeta KA, Coaker G (2015) PBL13 Is a serine/threonine protein kinase that negatively regulates Arabidopsis immune responses. *Plant Physiol* 169: 2950-2962

Loytynoja A, Vilella AJ, Goldman N (2012) Accurate extension of multiple sequence alignments using a phylogeny-aware graph algorithm. *Bioinformatics* 28: 1684-91

MacLean B, Tomazela DM, Shulman N, Chambers M, Finney GL, Frewen B, Kern R, Tabb DL, Liebler DC, MacCoss MJ (2010) Skyline: an open source document editor for creating and analyzing targeted proteomics experiments. *Bioinformatics* 26: 966-968

Meitzler JL, Antony S, Wu Y, Juhasz A, Liu H, Jiang G, Lu J, Roy K, Doroshow JH (2014) NADPH oxidases: a perspective on reactive oxygen species production in tumor biology. *Antioxid Redox Signal* 20: 2873-2889

Nakagami H (2014) StageTip-based HAMMOC, an efficient and inexpensive phosphopeptide enrichment method for plant shotgun phosphoproteomics. *Methods Mol Biol* 1072: 595-607

Ogasawara Y, Kaya H, Hiraoka G, Yumoto F, Kimura S, Kadota Y, Hishinuma H, Senzaki E, Yamagoe S, Nagata K, Nara M, Suzuki K, Tanokura M, Kuchitsu K (2008) Synergistic activation of the Arabidopsis NADPH oxidase AtrbohD by Ca^{2+} and phosphorylation. *J Biol Chem* 283: 8885-8892

Pandey D, Gratton JP, Rafikov R, Black SM, Fulton DJ (2011) Calcium/calmodulin-dependent kinase II mediates the phosphorylation and activation of NADPH oxidase 5. *Mol Pharmacol* 80: 407-415

Price MN, Dehal PS, Arkin AP (2010) FastTree 2--approximately maximum-likelihood trees for large alignments. *PLoS One* 5: e9490

Raad H, Paclet MH, Boussetta T, Kroviarski Y, Morel F, Quinn MT, Gougerot-Pocidalo MA, Dang PM, El-Benna J (2009) Regulation of the phagocyte NADPH oxidase activity: phosphorylation of $gp91^{phox}$/NOX2 by protein kinase C enhances its diaphorase activity and binding to Rac2, $p67^{phox}$, and $p47^{phox}$. *FASEB J* 23: 1011-1022

Schmidt R, Kunkowska AB, Schippers JH (2016) Role of reactive oxygen species during cell expansion in leaves. *Plant Physiol* 172: 2098-2106

Shiu SH, Bleecker AB (2001) Plant receptor-like kinase gene family: diversity, function, and signaling. *Sci STKE* 2001: re22

Siligato R, Wang X, Yadav SR, Lehesranta S, Ma G, Ursache R, Sevilem I, Zhang J, Gorte M, Prasad K, Wrzaczek M, Heidstra R, Murphy A, Scheres B, Mahonen AP (2016) MultiSite gateway-compatible cell type-specific gene-inducible system for plants. *Plant Physiol* 170: 627-641

Stamatakis A (2014) RAxML version 8: a tool for phylogenetic analysis and post-analysis of large phylogenies. *Bioinformatics* 30: 1312-1313

Stone JM, Walker JC (1995) Plant protein kinase families and signal transduction. *Plant Physiol* 108: 451-457

Sugiyama N, Masuda T, Shinoda K, Nakamura A, Tomita M, Ishihama Y (2007) Phosphopeptide enrichment by aliphatic hydroxy acid-modified metal oxide chromatography for nano-LC-MS/MS in proteomics applications. *Mol Cell Proteomics* 6: 1103-1109

Suzuki N, Miller G, Morales J, Shulaev V, Torres MA, Mittler R (2011) Respiratory burst oxidases: the engines of ROS signaling. *Curr Opin Plant Biol* 14: 691-699

Tanaka H, Osakabe Y, Katsura S, Mizuno S, Maruyama K, Kusakabe K, Mizoi J, Shinozaki K, Yamaguchi-Shinozaki K (2012) Abiotic stress-inducible receptor-like kinases negatively control ABA signaling in Arabidopsis. *Plant J* 70: 599-613

780 Torres MA, Dangl JL, Jones JD (2002) Arabidopsis gp91^{phox} homologues *AtrbohD* and *AtrbohF* are required
781 for accumulation of reactive oxygen intermediates in the plant defense response. *Proc Natl Acad Sci USA* 99:
782 517-522
783 Toyota M, Spencer D, Sawai-Toyota S, Wang J, Zhang T, Koo AJ, Howe GA, Gilroy S (2018) Glutamate
784 triggers long-distance, calcium-based plant defense signaling. *Science* 361: 1112-1115
785 Vaattovaara A, Brandt B, Rajaraman S, Safronov O, Veidenberg A, Luklova M, Kangasjarvi J, Loytynoja A,
786 Hothorn M, Salojarvi J, Wrzaczek M (2019) Mechanistic insights into the evolution of DUF26-containing
787 proteins in land plants. *Commun Biol* 2: 56
788 Waszczak C, Carmody M, Kangasjärvi J (2018) Reactive oxygen species in plant signaling. *Annu Rev Plant*
789 *Biol* 69: 209-236
790 Veidenberg A, Medlar A, Löytynoja A (2016) Wasabi: An integrated platform for evolutionary sequence
791 analysis and data visualization. *Mol Biol Evol* 33: 1126-1130
792 Veronese P, Nakagami H, Bluhm B, Abuqamar S, Chen X, Salmeron J, Dietrich RA, Hirt H, Mengiste T
793 (2006) The membrane-anchored *BOTRYTIS-INDUCED KINASE1* plays distinct roles in *Arabidopsis*
794 resistance to necrotrophic and biotrophic pathogens. *Plant Cell* 18: 257-273
795 Whalen MC, Innes RW, Bent AF, Staskawicz BJ (1991) Identification of *Pseudomonas syringae* pathogens
796 of *Arabidopsis* and a bacterial locus determining avirulence on both *Arabidopsis* and soybean. *Plant Cell* 3:
797 49-59
798 Wrzaczek M, Brosché M, Salojärvi J, Kangasjärvi S, Idänheimo N, Mersmann S, Robatzek S, Karpinski S,
799 Karpinska B, Kangasjärvi J (2010) Transcriptional regulation of the CRK/DUF26 group of receptor-like
800 protein kinases by ozone and plant hormones in Arabidopsis. *BMC Plant Biol* 10: 95
801 Wrzaczek M, Rozhon W, Jonak C (2007) A Proteasome-regulated glycogen synthase kinase-3 modulates
802 disease response in plants. *J Biol Chem* 282: 5249-5255
803 Yadeta KA, Elmore JM, Creer AY, Feng B, Franco JY, Rufian JS, He P, Phinney B, Coaker G (2017) A
804 cysteine-rich protein kinase associates with a membrane immune complex and the cysteine residues are
805 required for cell death. *Plant Physiol* 173: 771-787
806 Yeh YH, Chang YH, Huang PY, Huang JB, Zimmerli L (2015) Enhanced Arabidopsis pattern-triggered
807 immunity by overexpression of cysteine-rich receptor-like kinases. *Front Plant Sci* 6: 322
808 Yeh YH, Panzeri D, Kadota Y, Huang YC, Huang PY, Tao CN, Roux M, Chien HC, Chin TC, Chu PW,
809 Zipfel C, Zimmerli L (2016) The Arabidopsis Malectin-Like/LRR-RLK IOS1 Is Critical for BAK1-
810 Dependent and BAK1-Independent Pattern-Triggered Immunity. *Plant Cell* 28: 1701-21
811 Yun BW, Feechan A, Yin M, Saidi NB, Le Bihan T, Yu M, Moore JW, Kang JG, Kwon E, Spoel SH, Pallas
812 JA, Loake GJ (2011) S-nitrosylation of NADPH oxidase regulates cell death in plant immunity. *Nature* 478:
813 264-268
814 Zhang J, Shao F, Li Y, Cui H, Chen L, Li H, Zou Y, Long C, Lan L, Chai J, Chen S, Tang X, Zhou JM
815 (2007) A Pseudomonas syringae effector inactivates MAPKs to suppress PAMP-induced immunity in plants.
816 *Cell Host Microbe* 1: 175-85
817 Zhang M, Chiang YH, Toruno TY, Lee D, Ma M, Liang X, Lal NK, Lemos M, Lu YJ, Ma S, Liu J, Day B,
818 Dinesh-Kumar SP, Dehesh K, Dou D, Zhou JM, Coaker G (2018) The MAP4 kinase SIK1 ensures robust
819 extracellular ROS burst and antibacterial immunity in plants. *Cell Host Microbe* 24: 379-391
820 Zipfel C, Robatzek S, Navarro L, Oakeley EJ, Jones JD, Felix G, Boller T (2004) Bacterial disease resistance
821 in *Arabidopsis* through flagellin perception. *Nature* 428: 764-767

Figure legends:

Fig. 1 CRK2 kinase activity is required for plant growth.

a Schematic representation of CRK2 structure. SP: signal peptide (AAs 1-29), DUF26-A (AAs 39-132), DUF26-B (AAs 146-243), TM: transmembrane domain (AAs 261-283), and kinase domain (AAs 325-601).

b Representative pictures of 21-day-old plants of Col-0, *crk2*, *CRK2pro::CRK2-YFP/crk2*, *CRK2pro::CRK2*^{K353E}*-YFP/crk2* and *CRK2pro::CRK2*^{D450N}*-YFP/crk2* plants. Bar = 1 cm.

c Box plot shows the fresh weight of 21-day-old plants (n = 10). Differences between Col-0 and transgenic lines were evaluated with One-way Anova with Tukey-Kramer HSD, *** $p<0.001$, ns, not statistically significant (Oneway Anova, F value = 71.5559, DF = 7). The experiment was repeated three times with similar results.

Fig. 2 CRK2 regulates flg22-triggered ROS production and resistance to a virulent bacterial pathogen.

a and **b** flg22-induced ROS production in Col-0, *crk2* and *CRK2pro::CRK2-YFP/crk2* or *CRK2pro::CRK2*^{D450N}*-YFP/crk2*. Leaf discs from 28-day-old plants were treated with 200 nM flg22 and ROS production was measured. Box plot shows cumulative ROS production over 40 min (upper right).

a Values represent mean ±SEM of $n \geq 16$. Differences compared with Col-0 were evaluated with One-way Anova (F value = 9.2282, DF = 3) with Tukey-Kramer HSD, *** $p < 0.001$, ns, not statistically significant.

b Values represent the mean ±SEM of $n \geq 19$. Differences compared with Col-0 were evaluated with One-way Anova (F value = 8.8777, DF = 3) with Tukey-Kramer HSD, *$p < 0.05$, *** $p < 0.001$.

c Quantitative analysis of bacterial growth in Col-0, *crk2* and *CRK2pro::CRK2-YFP/crk2 or CRK2pro::CRK2*^{D450N}*-YFP/crk2* following syringe infiltration with *Pto* DC3000 (1 x 10^5 CFU/mL). Values represent mean ±SD of n = 3 (0 DPI) or n = 6 (2 DPI). Letters indicate significant differences at $p < 0.05$ [One-way Anova (F value = 566.5661, DF = 11) with Tukey-Kramer HSD]. **a** - **c** The experiment was repeated three times with similar results.

Fig. 3 CRK2 interacts with RBOHD.

a ROS production of RBOHD-expressing HEK293T cells. 3FLAG-RBOHD was transiently co-expressed with either 3Myc-GFP or CRK2 (WT or D450N)-3Myc. After 30 min 1 µM ionomycin was added to the medium. Values represent mean ±SEM of n = 3. E.V. = empty vector. The experiment was repeated three times with similar results.

b and **c** Co-IP analysis of interaction between RBOHD and CRK2. CRK2-YFP was immuno-precipitated using anti-GFP beads followed by immunoblotting with anti-RBOHD and anti-GFP antibodies. FLAG-RBOHD: 105 kDa, CRK2-YFP: 99.9 kDa and YFP-6Myc: 36.7 kDa.

b *35S::FLAG-RBOHD/rbohD x 35S::CRK2-YFP/Col-0* (F1) and *35S::FLAG-RBOHD/rbohD x 35S::YFP-6Myc/Col-0* (F1) plants. The experiment was repeated three times with similar results.

c *35S::FLAG-RBOHD/35S::CRK2-YFP/rbohD* plants with 1 µM flg22 treatment. M: Protein molecular marker, *: unspecific signal. Total protein from *rbohD* was used for immunoblot of input as a negative control.

d Schematic representation of RBOHD structure. EF-hands (AAs 257-329), TM: transmembrane domains (AAs 374 - 605), FAD: FAD-binding domain (AAs 613-730), NADPH: NADPH-binding domain (AAs 736-904), RBOHD/N: RBOHD N-terminal region (AAs 1-376), RBOHD/C: RBOHD C-terminal region (AAs 606-922); C1: RBOHD/C1 (AAs 606-741), C2: RBOHD/C2 (AAs 696-831), C3: RBOHD/C3 (AAs 787-922).

e *In vitro* pull-down analysis of direct interaction between RBOHD and CRK2. MBP, 6His-MBP-RBOHD/N and 6His-MBP-RBOHD/C were incubated with 6His-GST-CRK2cyto and pull down with GST followed by immunoblotting with anti-6His and anti-MBP antibodies. 6His-GST-CRK2cyto: 68.5 kDa, 6His-MBP-RBOHD/N: 84.7 kDa, 6His-MBP-RBOHD/C: 78.4 kDa, MBP: 50.8 kDa. The experiment was repeated two times with similar results.

Fig. 4 CRK2 phosphorylates the cytosolic regions of RBOHD *in vitro*.

a and **b** Autophosphorylation and transphosphorylation were visualized with [γ-^{32}P] ATP and autoradiography (upper panel). Input proteins were stained with coomassie brilliant blue (CBB) (lower panel). Experiments were repeated three times with similar results. 6His-GST-CRK2cyto: 68.5 kDa, 6His-MBP-RBOHD/N: 84.7 kDa, 6His-MBP-RBOHD/C1:57.9 kDa, /C2:57.8 kDa, /C3:58.4 kDa, 6His-MBP: 44.3 kDa.

a *In vitro* transphosphorylation of 6His-MBP-RBOHD N-terminus by 6His-GST-CRK2cyto. 6His-MBP-RBOHD/N or 6His-MBP was incubated with 6His-GST-CRK2cyto in kinase buffer.

b *In vitro* transphosphorylation of 6His-MBP-RBOHD C-terminus by 6His-GST-CRK2cyto. 6His-MBP-RBOHD/C1, /C2, /C3 or 6His-MBP was incubated with 6His-GST-CRK2cyto in kinase buffer.

Fig. 5 CRK2 modulates the ROS-production activity of RBOHD *via* phosphorylation of the C-terminus in HEK293T cells.

a Effect of mutations of CRK2-dependent *in vitro* phosphorylation sites in the N-terminal cytosolic region of RBOHD. 3FLAG-RBOHD (WT, S8A or S39A) was transiently co-expressed with either 3Myc-GFP or CRK2-3Myc in HEK293T cells. After 30 min 1 µM ionomycin was added to the medium to promote Ca^{2+}

887 influx. Values represent mean ±SEM of n = 3. E.V. = empty vector. The experiment was repeated three times
888 with similar results.

889 **b** Effect of mutations in the CRK2-dependent *in vitro* phosphorylation sites in the C-terminal cytosolic
890 region of RBOHD. 3FLAG-RBOHD (WT, S611A, S703A or S862A) were transiently co-expressed with
891 either 3Myc-GFP or CRK2-3Myc in HEK293T cells. After 30 min 1 µM ionomycin was added to the
892 medium to promote Ca^{2+} influx. Values represent mean ±SEM of n = 3. E.V. = empty vector. The
893 experiment was repeated three times with similar results.

894

895 **Fig. 6 RBOHD S703 is involved in regulation of flg22-induced ROS production.**
896 **a - c** Quantification of RBOHD phosphorylation in Col-0 upon flg22 treatment. 12-day-old seedlings were
897 treated with water (-) or 1 µM flg22 (+) for 5 min. Total proteins were digested with trypsin (S8 and S39) or
898 Lys-C (S703) and phosphopeptides were enriched, and then selected phosphopeptides were quantified by
899 LC-MS/MS. Box plots show MS2 fragment peak ion areas of indicated phosphopeptides (n = 4). Differences
900 between water- or flg22-treated samples were evaluated with One-way Anova (DF = 1) with Tukey-Kramer
901 HSD, *** $p<0.001$, ns, not statistically significant.

902 **a** RBOHD S8 residue (F value = 0.4745).

903 **b** RBOHD S39 residue (F value = 51.3297).

904 **c** RBOHD S703 residue (F value = 41.0851).

905 **d** flg22-induced ROS production in *RBOHDpro::3FLAG-RBOHD/rbohD* #1-3 and *RBOHDpro::3FLAG-*
906 *RBOHD*^{S703A}*/rbohD* #3-2. Leaf discs from 28-day-old plants were treated with 200 nM flg22. Box plot shows
907 cumulative ROS production over 40 min (upper right). Values represent mean ±SEM of $n \geq 23$. Difference
908 between lines was evaluated with One-way Anova (F value = 4.4509, DF = 1) with Tukey-Kramer HSD, * $p < 0.05$. The experiment was repeated three times with similar results.

910

911 **Fig. 7 Phosphorylation sites in the C-terminal region are conserved in plants and animals.**
912 Phylogenetic tree showing that plant RBOHs form a single clade which is parallel to the NADPH oxidases
913 NOX2 and NOX5β from *Homo sapiens*. The tree was constructed using FASTTREE from a PAGAN
914 alignment in WASABI, 1000 bootstraps were calculated with RAxML. The full sequence alignment can be
915 found in Wasabi at http://was.bi?id=JauZ6q. Plant species included were: *Arabidopsis thaliana* (*At*),
916 *Capsella rubella* (*Cr*), *Prunus persica* (*Pp*), *Solanum lycopersicum* (*Sl*), *Aquilegia coerula* (*Ac*), *Oryza sativa*
917 (*Os*), *Sorghum bicolor* (*Sb*), *Amborella trichopoda* (*Atr*), and *Marchantia polymorpha* (*Mp*). Numbers of
918 phospho-sites in the meme figures represent the position of the amino acid in RBOHD from *Arabdiopsis*
919 *thaliana*. Arrows indicate the position of the phospho-site (S or T) or corresponding amino acid.

Fig. 8 Schematic model for MAMP-triggered RBOHD activation.

MAMPs are recognized by MAMP receptor complexes. RBOHD N-terminus is phosphorylated by BIK1 and SIK1 and apoplastic ROS production is induced. Apoplastic ROS production by RBOHD leads to Ca^{2+} influx into the cytosol. Ca^{2+}-binding to RBOHD N-terminus and to CPKs leads to Ca^{2+}-dependent activation of RBOHD. We found that CRK2 also contributes to the activation of RBOHD *via* phosphorylation of its C-terminus at S703. CRK2 can also mediates inhibition of MAPK activation and callose deposition *via* CALS after MAMP perception. MPK, mitogen-activated protein kinase; MP2K, MPKK; MP3K, MPKKK.

Supplementary figure legends

Fig. S1 Complementation of *crk2* with *CRK2pro::CRK2-YFP*.

a Box plot shows dry weight of 21-day-old plants (n = 10). Differences compared with Col-0 were evaluated with One-way Anova with Tukey-Kramer HSD, *** $p < 0.001$, ns, not statistically significant (One-way Anova, F value = 48.2539, DF = 7). The experiment was repeated three times with similar results.

b Salicylic acid accumulation level in Col-0, *crk2* and *CRK2pro::CRK2-YFP/crk2 #1-22* (n = 3). 6-day-old seedlings were used. Differences compared with Col-0 were evaluated with One-way Anova (F value = 3.0476, DF = 2) with Tukey-Kramer HSD. ns, not statistically significant.

c Subcellular localization of CRK2-YFP, $CRK2^{K353E}$-YFP and $CRK2^{D450N}$-YFP in leaves of 7-day-old seedlings. Plasma membrane localization was confirmed using plasmolysis to visualize Hechtian strands (arrow head). Plasmolysis was induced by the application of 0.8 M mannitol. Scale bar = 25 µm.

Fig. S2 MAMP-triggered ROS production and molecular responses in *crk2*.

a and **b** Box plot shows quantitative real-time RT-PCR (qPCR) analysis of *FRK1* (a) or *NHL10* (b) transcripts in Col-0, *crk2* and *fls2* after treatment with flg22 (n = 3, biological replicates). 10-day-old plants were incubated in 1 µM flg22 solution and collected at indicated time (each time point contains 90 plants per genotype). Transcript levels were calculated by comparison with non-treated Col-0 (Time = 0).

a *FRK1* expression. Different letters indicate significant difference at $p < 0.05$ [One-way Anova (F value = 9.4471, DF = 11) with Tukey-Kramer HSD].

b *NHL10* expression. Different letters indicate significant difference at $p < 0.05$ [One-way Anova (F value = 9.1059, DF = 11) with Tukey-Kramer HSD].

c and **d** Chitin- or AtPep1- induced ROS production in Col-0, *crk2* and *rbohD*. Leaf discs from 28-day-old plants were treated with 200 µg/mL chitin (c) or 1 µM AtPep1 (d). ROS production is expressed in relative

952 luminescence units (RLU). Box plots show integration of ROS production for 40 min (upper right). The
953 experiment was repeated three times with similar results.

954 **c** Values represent the mean ±SEM of $n \geq 21$. Differences compared with Col-0 were evaluated with One-
955 way Anova (F value = 24.1435, DF = 2) with Tukey-Kramer HSD, * $p < 0.05$, *** $p < 0.001$.

956 **d** Values represent the mean ±SEM of $n = 24$. Differences compared with Col-0 were evaluated with One-
957 way Anova (F value = 44.5132, DF = 2) with Tukey-Kramer HSD, *** $p < 0.001$.

958 **e** Quantitative analysis of cytosolic Ca^{2+} changes in response to 1 µM flg22 in 7-day-old *YCNano65* or
959 *YCNano65/crk2* seedlings. Values represent the mean ±SEM of n = 9 (*YCNano65*) or n = 15
960 (*YCNano65/crk2*).

961 **f** Representative frame images of cytosolic Ca^{2+} change in wild type and *crk2* plants. Bar = 0.5 mm.

962 **g** MAPK activation in Col-0, *crk2* and *fls2* in response to treatment with 1 µM flg22. 28-day-old plants (12
963 plants per genotype). Phosphorylated MPK3 and MPK6 were detected with anti-p44/42 MPK antibody
964 (upper panel). Proteins stained with amido black staining (lower panel). The experiment was repeated three
965 times with similar results.

966 **h** Quantification of flg22-induced callose deposition by aniline blue ($n \geq 16$) in 7-day-old seedlings with (+)
967 or without (-) treatment with 10 µM flg22 for 30 min. Letters indicate significant differences at $p < 0.05$
968 [One-way Anova (F value = 44.8732, DF = 3) with Tukey-Kramer HSD].

969 **i** Representative images of aniline blue stained leaves. Bar = 100 µm.

970

971 **Fig. S3 CRK2 modulates the ROS-producing activity of RBOHC, D and F in HEK293T cells.**
972 **a** Expressed proteins were detected by anti-FLAG and anti-Myc antibodies (Fig. 3a). 3FLAG-RBOHD: 107
973 kDa, CRK2-3Myc: 75.8 kDa, 3Myc-GFP: 31 kDa, β-actin 42 kDa. As a loading control, β-actin was used.
974 Loading volume for anti-Myc antibody: 3FLAG-RBOHD + 3Myc-GFP (5 µL), the others (50 µL).

975 **b** ROS production in RBOHD-expressing HEK293T cells in Ca^{2+}-free buffer. 3FLAG-RBOHD was
976 transiently co-expressed with either 3Myc-GFP or 3Myc-CRK2 (WT or D450N) in HEK293T cells. Values
977 represent mean ±SEM of n = 3. E.V. = empty vector. The experiment was repeated three times with similar
978 results.

979 **c** Proteins expressed in HEK293T cells were detected by anti-FLAG and anti-Myc antibodies (Fig. S3b).
980 3FLAG-RBOHD: 107 kDa, CRK2-3Myc: 75.8 kDa, 3Myc-GFP: 31 kDa, β-actin 42 kDa. As a loading
981 control, β-actin was used. Loading volume for anti-Myc antibody: 3FLAG-RBOHD + 3Myc-GFP (5 µL),
982 others (50 µL).

d - f ROS production of RBOHD-, RBOHC-, or RBOHF-expressing HEK293T cells. 3FLAG-RBOHD (d), 3FLAG-RBOHC (e), or 3FLAG-RBOHF (f) was transiently co-expressed with 3Myc-GFP or CRK2-3Myc in HEK293T cells, respectively. After 20 min of base line measurement, 1 μM ionomycin was added to the medium. Values represent mean ±SEM of n = 3. The experiment was repeated two times with similar results.

g Proteins expressed in HEK293T cells were detected by anti-FLAG and anti-Myc antibodies (Fig. S3d-f). 3FLAG-RBOHD: 107 kDa, 3FLAG-RBOHC, 106 kDa, 3FLAG-RBOHF: 111 kDa, CRK2-3Myc: 75.8 kDa, 3Myc-GFP: 31 kDa, β-actin 42 kDa. As a loading control, β-actin was used. Loading volume for anti-Myc antibody: 3FLAG-RBOHs + 3Myc-GFP (5 μL), 3FLAG-RBOHs + CRK2-3Myc (50 μL).

Fig. S4 ROS production activity of RBOHD S703A and S862A in HEK293T cells.

a and **b** Proteins expressed in HEK293T cells were detected by anti-FLAG and anti-Myc antibodies (Fig. 5a and 5b). 3FLAG-RBOHD: 107 kDa, CRK2-3Myc: 75.8 kDa, 3Myc-GFP: 31 kDa, β-actin 42 kDa. As a loading control, β-actin was used. Loading volume for anti-Myc antibody: 3FLAG-RBOHD + 3Myc-GFP (5 μL), others (50 μL).

a 3FLAG-RBOHD (WT, S8A or S39A) was transiently co-expressed with either 3Myc-GFP or CRK2-3Myc into HEK293T cells (Fig. 5a).

b 3FLAG-RBOHD (WT, S611A, S703A or S862A) was transiently co-expressed with either 3Myc-GFP or CRK2-3Myc into HEK293T cells (Fig. 5b).

c and **d** ROS production of RBOHD-expressing HEK293T cells. After 30 min 1 μM ionomycin was added to the medium. Values represent mean ±SEM of n = 3. E.V. = empty vector. The experiment was repeated three times with similar results.

c 3FLAG-RBOHD (WT or S703A) was transiently co-expressed with either 3Myc-GFP or CRK2-3Myc into HEK293T cells. The right upper panel is the enlargement of ionomycin-induced transient ROS production of 3FLAG-RBOHD (WT or S703A) and 3Myc-GFP co-expressing cells (dashed box).

d 3FLAG-RBOHD (WT or S862A) was transiently co-expressed with either 3Myc-GFP or CRK2-3Myc into HEK293T cells.

Fig. S5 Quantification of RBOHD and MPK phosphorylation in Col-0 upon flg22 treatment.

12-day-old Col-0 seedlings were treated with water (-) or 1 μM flg22 (+) for 5 min. Total proteins were digested by trypsin for peptides from RBOHD N-terminal region and MPKs, by Lys-C for RBOHD S703 peptide. Peptides were enriched, and then selected phosphopeptides were quantified by LC-MS/MS. Box plots show MS2 fragment peak ion areas of indicated phosphopeptides (n = 4). Differences between water-

or flg22-treated samples were evaluated with One-way Anova (DF = 1) with Tukey-Kramer HSD, * P<0.05, ** P<0.01, *** p<0.001, ns, not statistically significant.

a and **b** RBOHD S8 residue [F value = 9.3550 (a), F value = 1.7274 (b)].

c RBOHD S39 residue (F value = 51.1741).

d RBOHD S703 residue (F value = 87.8835).

e RBOHD S163 residue (F value = 71.8320).

f RBOHD S347 residue (F value = 22.8032).

g RBOHD S343 and S347 residues (F value = 10.9184).

h MPK3 TEY motif (F value = 8.0906).

i MPK6 TEY motif (F value = 33.9863).

j MPK11 TEY motif (F value = 11.6362).

Fig. S6 RBOHD S703 is involved in regulation of flg22-induced ROS production.

a Representative pictures of 21-day-old plants of *RBOHDpro::3FLAG-RBOHD/rbohD* #1-3 and *RBOHDpro::3FLAG-RBOHD*^{S703A}*/rbohD* #3-2 plants. Bar = 1 cm.

b Expressed proteins in *RBOHDpro::3FLAG-RBOHD/rbohD* #1-3 and *RBOHDpro::3FLAG-RBOHD*^{S703A}*/rbohD* #3-2. 3FLAG-RBOHD was detected by anti-FLAG antibody. Input proteins stained with amido black staining (lower panel).

c flg22-induced ROS production in *RBOHDpro::3FLAG-RBOHD/rbohD* #11-1 and *RBOHDpro::3FLAG-RBOHD*^{S703A}*/rbohD* #1-4. Leaf discs from 28-day-old plants were treated with 200 nM flg22. Box plots show integration of ROS production for 40 min (upper right). Values represent the mean ±SEM of n = 24. Difference between lines was evaluated with One-way Anova (F value = 15.4533, DF = 1) with Tukey-Kramer HSD, *** p < 0.001.

Fig. S7 Reduced ROS production in *crk2* is not due to lower expression of *BIK1*.

Box plot shows quantitative real-time RT-PCR (qPCR) analysis of *BIK1* transcripts in Col-0, *crk2* and *fls2* after treatment with flg22 (n = 3, biological replicates). 10-day-old plants were incubated in 1 µM flg22 solution and collected at indicated time (each time point contains 90 plants per genotype). Transcript levels were calculated by comparison with non-treated Col-0 (Time = 0). Different letters indicate significant difference at p < 0.05 [One-way Anova (F value = 220.6240, DF = 8) with Tukey-Kramer HSD].

Supplementary table legends

Table S1. *In vitro* phosphorylation sites of 6His-MBP-RBOHDcyto by 6His-GST-CRK2cyto

The 6His-MBP-RBOHD cytosolic regions were incubated with 6His-GST-CRK2cyto. The 6His-MBP-RBOHDcyto bands were excised from a SDS polyacrylamide gel and subsequently digested by trypsin or Lys-C. The peptides were analyzed by LC-MS/MS. Phosphorylated peptides are designated as pS.

Table S2. Progeny of *CRK2/crk2 BIK1/bik1* parent and *CRK2/crk2 bik1/bik1* parent

The genotypes of F2 and F3 progenies were determined by PCR. Observed, the number of individuals observed; Expected, the expected number based on Mendelian inheritance. Chi-square test was used to determine the probability (P) of which the deviation of the observed value from the expected value was due to chance.

Table S3. Primer sequences

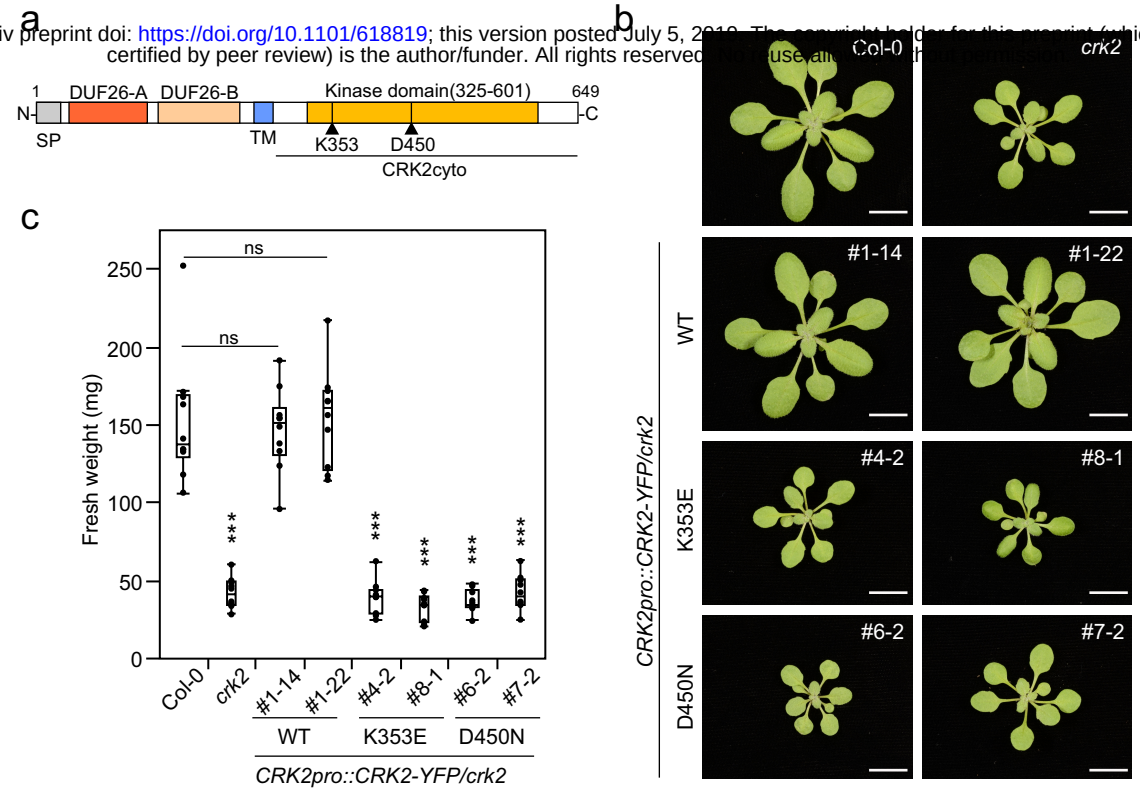

Fig. 1 CRK2 kinase activity is required for plant growth.

a Schematic representation of CRK2 structure. SP: signal peptide (AAs 1-29), DUF26-A (AAs 39-132), DUF26-B (AAs 146-243), TM: transmembrane domain (AAs 261-283), and kinase domain (AAs 325-601).

b Representative pictures of 21-day-old plants of Col-0, *crk2, CRK2pro::CRK2-YFP/crk2, CRK2pro::CRK2*^{K353E}*-YFP/crk2 and CRK2pro::CRK2*^{D450N}*-YFP/crk2* plants. Bar = 1 cm.

c Box plot shows the fresh weight of 21-day-old plants (n = 10). Differences between Col-0 and transgenic lines were evaluated with One-way Anova with Tukey-Kramer HSD, *** $p<0.001$, ns, not statistically significant (Oneway Anova, F value = 71.5559, DF = 7). The experiment was repeated three times with similar results.

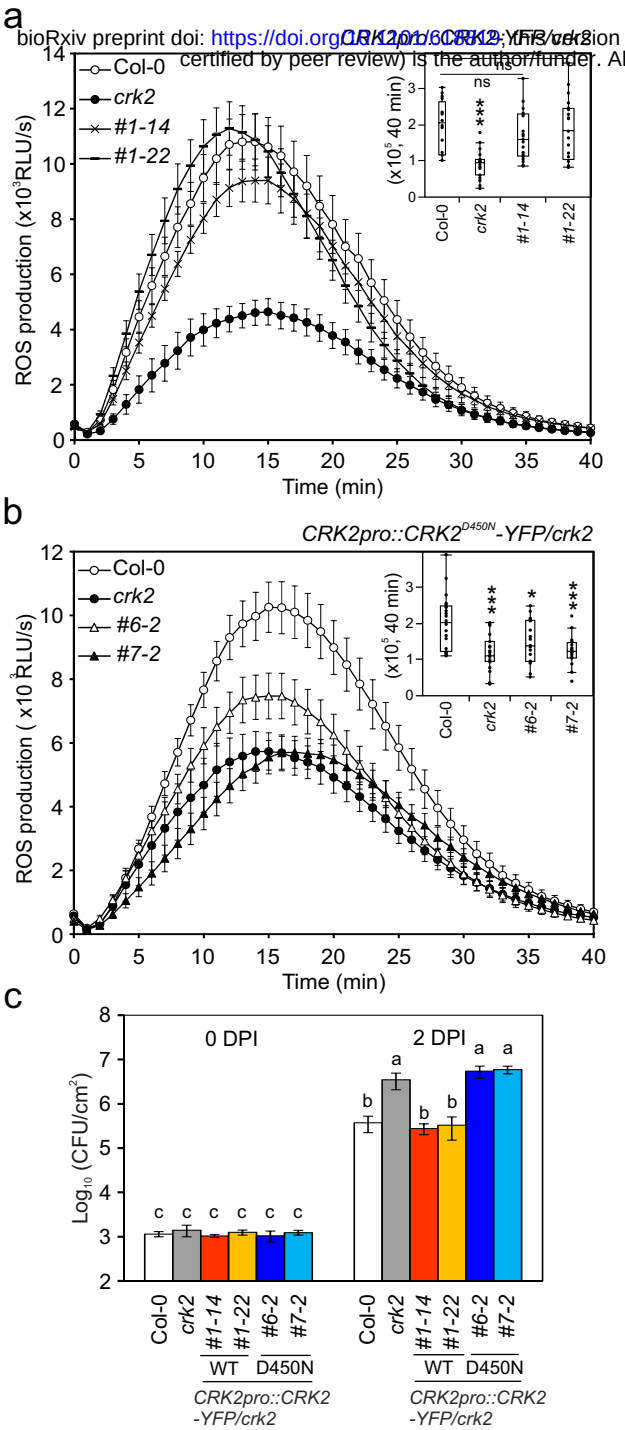

Fig. 2 CRK2 regulates flg22-triggered ROS production and resistance to a virulent bacterial pathogen.

a and **b** flg22-induced ROS production in Col-0, *crk2* and *CRK2pro::CRK2-YFP/crk2* or *CRK2pro::CRK2^{D450N}-YFP/crk2*. Leaf discs from 28-day-old plants were treated with 200 nM flg22 and ROS production was measured. Box plot shows cumulative ROS production over 40 min (upper right).

a Values represent mean ±SEM of n ≥ 16. Differences compared with Col-0 were evaluated with One-way Anova (F value = 9.2282, DF = 3) with Tukey-Kramer HSD, *** p < 0.001, ns, not statistically significant.

b Values represent the mean ±SEM of n ≥ 19. Differences compared with Col-0 were evaluated with One-way Anova (F value = 8.8777, DF = 3) with Tukey-Kramer HSD, *p < 0.05, *** p < 0.001.

c Quantitative analysis of bacterial growth in Col-0, *crk2* and *CRK2pro::CRK2-YFP/crk2 or CRK2pro::CRK2^{D450N}-YFP/crk2* following syringe infiltration with *Pto* DC3000 (1 x 10^5 CFU/mL). Values represent mean ±SD of n = 3 (0 DPI) or n = 6 (2 DPI). Letters indicate significant differences at p < 0.05 [One-way Anova (F value = 566.5661, DF = 11) with Tukey-Kramer HSD]. **a** - **c** The experiment was repeated three times with similar results.

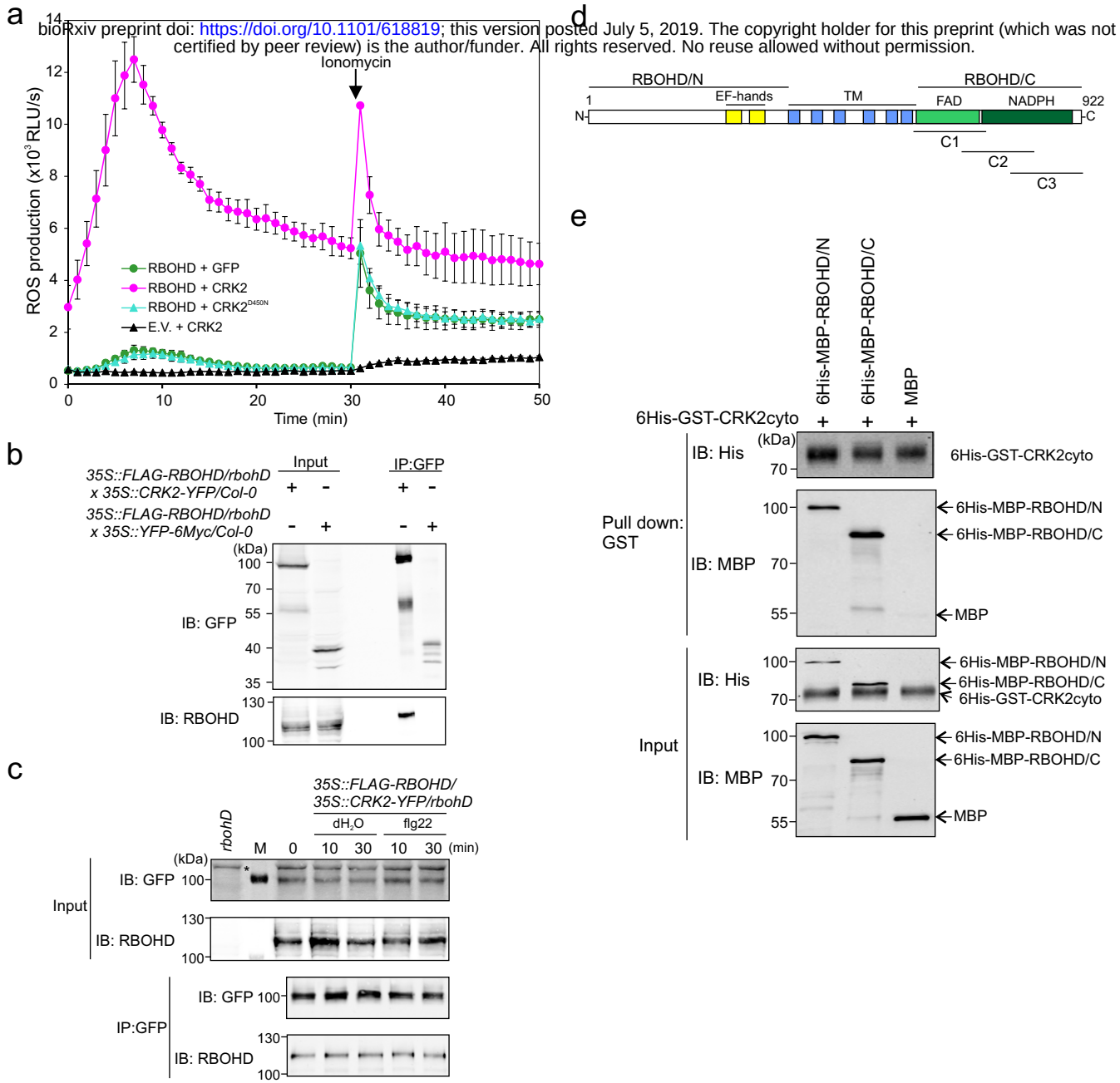

Fig. 3 CRK2 interacts with RBOHD.

a ROS production of RBOHD-expressing HEK293T cells. 3FLAG-RBOHD was transiently co-expressed with either 3Myc-GFP or CRK2 (WT or D450N)-3Myc. After 30 min 1 µM ionomycin was added to the medium. Values represent mean ±SEM of n = 3. E.V. = empty vector. The experiment was repeated three times with similar results.

b and **c** Co-IP analysis of interaction between RBOHD and CRK2. CRK2-YFP was immuno-precipitated using anti-GFP beads followed by immunoblotting with anti-RBOHD and anti-GFP antibodies. FLAG-RBOHD: 105 kDa, CRK2-YFP: 99.9 kDa and YFP-6Myc: 36.7 kDa.

b *35S::FLAG-RBOHD/rbohD x 35S::CRK2-YFP/Col-0* (F1) and *35S::FLAG-RBOHD/rbohD x 35S::YFP-6Myc/Col-0* (F1) plants. The experiment was repeated three times with similar results.

c *35S::FLAG-RBOHD/35S::CRK2-YFP/rbohD* plants with 1 µM flg22 treatment. M: Protein molecular marker, *: unspecific signal. Total protein from *rbohD* was used for immunoblot of input as a negative control.

d Schematic representation of RBOHD structure. EF-hands (AAs 257-329), TM: transmembrane domains (AAs 374 - 605), FAD: FAD-binding domain (AAs 613-730), NADPH: NADPH-binding domain (AAs 736-904), RBOHD/N: RBOHD N-terminal region (AAs 1-376), RBOHD/C: RBOHD C-terminal region (AAs 606-922); C1: RBOHD/C1 (AAs 606-741), C2: RBOHD/C2 (AAs 696-831), C3: RBOHD/C3 (AAs 787-922).

e *In vitro* pull-down analysis of direct interaction between RBOHD and CRK2. MBP, 6His-MBP-RBOHD/N and 6His-MBP-RBOHD/C were incubated with 6His-GST-CRK2cyto and pull down with GST followed by immunoblotting with anti-6His and anti-MBP antibodies. 6His-GST-CRK2cyto: 68.5 kDa, 6His-MBP-RBOHD/N: 84.7 kDa, 6His-MBP-RBOHD/C: 78.4 kDa, MBP: 50.8 kDa. The experiment was repeated two times with similar results.

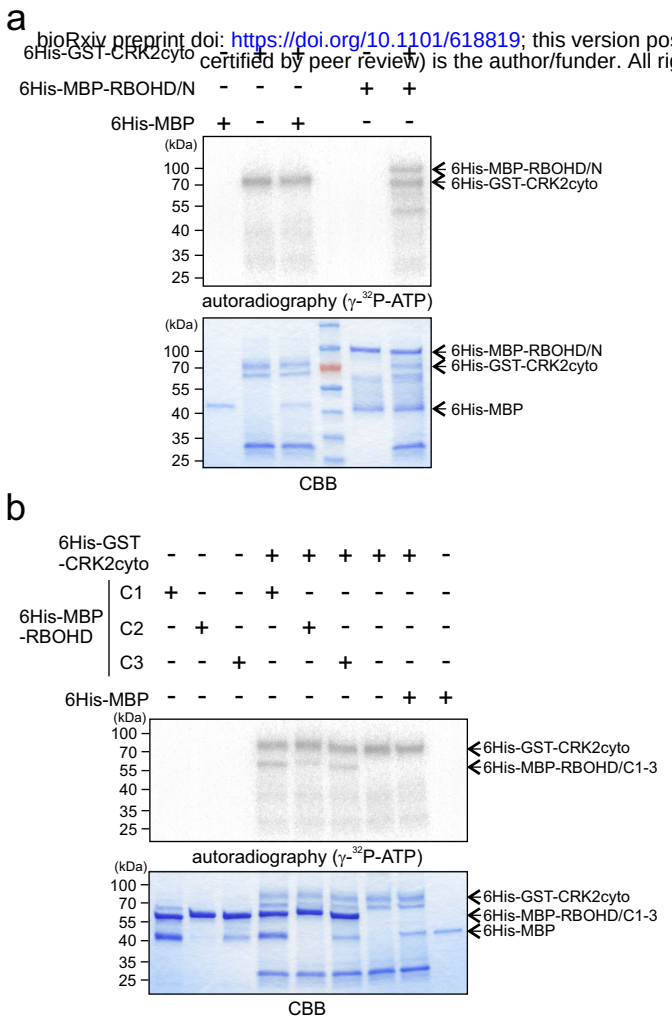

Fig. 4 CRK2 phosphorylates the cytosolic regions of RBOHD *in vitro*.

a and **b** Autophosphorylation and transphosphorylation were visualized with [γ-^{32}P] ATP and autoradiography (upper panel). Input proteins were stained with coomassie brilliant blue (CBB) (lower panel). Experiments were repeated three times with similar results. 6His-GST-CRK2cyto: 68.5 kDa, 6His-MBP-RBOHD/N: 84.7 kDa, 6His-MBP-RBOHD/C1:57.9 kDa, /C2:57.8 kDa, /C3:58.4 kDa, 6His-MBP: 44.3 kDa.

a *In vitro* transphosphorylation of 6His-MBP-RBOHD N-terminus by 6His-GST-CRK2cyto. 6His-MBP-RBOHD/N or 6His-MBP was incubated with 6His-GST-CRK2cyto in kinase buffer.

b *In vitro* transphosphorylation of 6His-MBP-RBOHD C-terminus by 6His-GST-CRK2cyto. 6His-MBP-RBOHD/C1, /C2, /C3 or 6His-MBP was incubated with 6His-GST-CRK2cyto in kinase buffer.

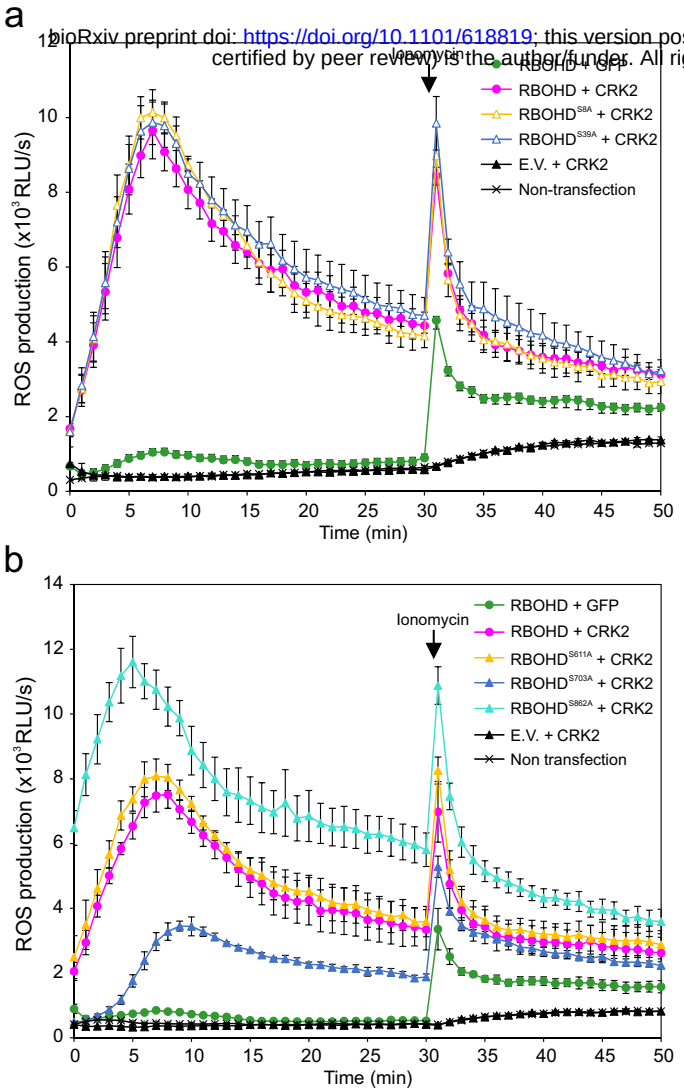

Fig. 5 CRK2 modulates the ROS-production activity of RBOHD *via* phosphorylation of the C-terminus in HEK293T cells.

a Effect of mutations of CRK2-dependent *in vitro* phosphorylation sites in the N-terminal cytosolic region of RBOHD. 3FLAG-RBOHD (WT, S8A or S39A) was transiently co-expressed with either 3Myc-GFP or CRK2-3Myc in HEK293T cells. After 30 min 1 μM ionomycin was added to the medium to promote Ca^{2+} influx. Values represent mean ±SEM of n = 3. E.V. = empty vector. The experiment was repeated three times with similar results.

b Effect of mutations in the CRK2-dependent *in vitro* phosphorylation sites in the C-terminal cytosolic region of RBOHD. 3FLAG-RBOHD (WT, S611A, S703A or S862A) were transiently co-expressed with either 3Myc-GFP or CRK2-3Myc in HEK293T cells. After 30 min 1 μM ionomycin was added to the medium to promote Ca^{2+} influx. Values represent mean ±SEM of n = 3. E.V. = empty vector. The experiment was repeated three times with similar results.

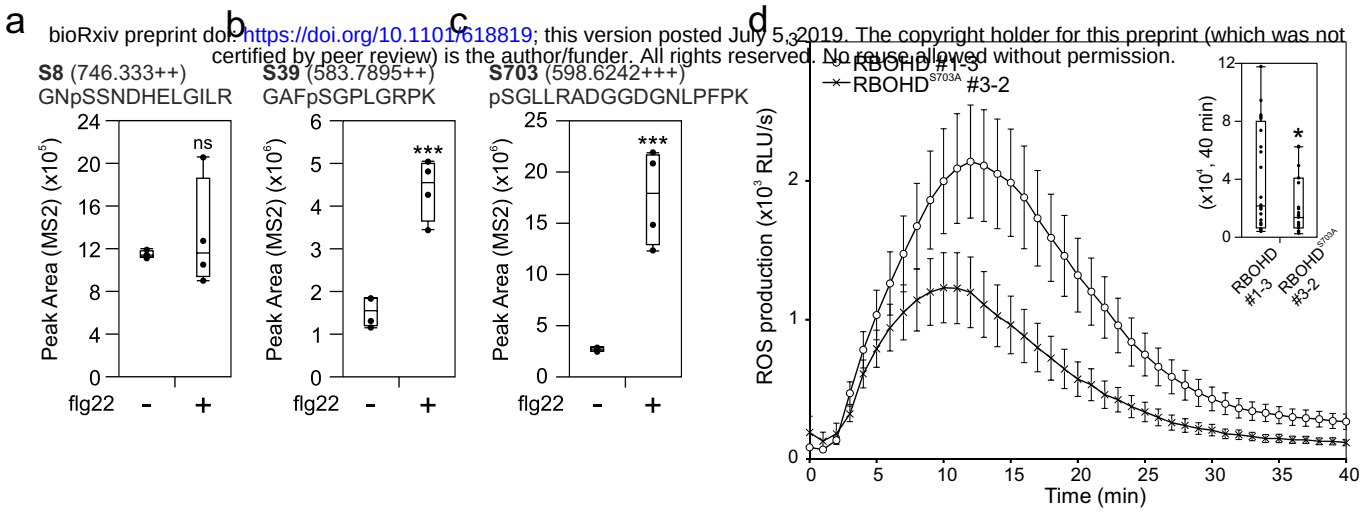

Fig. 6 RBOHD S703 is involved in regulation of flg22-induced ROS production.

a - **c** Quantification of RBOHD phosphorylation in Col-0 upon flg22 treatment. 12-day-old seedlings were treated with water (-) or 1 µM flg22 (+) for 5 min. Total proteins were digested with trypsin (S8 and S39) or Lys-C (S703) and phosphopeptides were enriched, and then selected phosphopeptides were quantified by LC-MS/MS. Box plots show MS2 fragment peak ion areas of indicated phosphopeptides (n = 4). Differences between water- or flg22-treated samples were evaluated with One-way Anova (DF = 1) with Tukey-Kramer HSD, *** $p<0.001$, ns, not statistically significant.

a RBOHD S8 residue (F value = 0.4745).

b RBOHD S39 residue (F value = 51.3297).

c RBOHD S703 residue (F value = 41.0851).

d flg22-induced ROS production in *RBOHDpro::3FLAG-RBOHD/rbohD* #1-3 and *RBOHDpro::3FLAG-RBOHD^{S703A}/rbohD* #3-2. Leaf discs from 28-day-old plants were treated with 200 nM flg22. Box plot shows cumulative ROS production over 40 min (upper right). Values represent mean ±SEM of $n \geq 23$. Difference between lines was evaluated with One-way Anova (F value = 4.4509, DF = 1) with Tukey-Kramer HSD, * $p < 0.05$. The experiment was repeated three times with similar results.

Fig. 7 Phosphorylation sites in the C-terminal region are conserved in plants and animals.
Phylogenetic tree showing that plant RBOHs form a single clade which is parallel to the NADPH oxidases NOX2 and NOX5β from *Homo sapiens*. The tree was constructed using FASTTREE from a PAGAN alignment in WASABI, 1000 bootstraps were calculated with RAxML. The full sequence alignment can be found in Wasabi at http://was.bi?id=JauZ6q. Plant species included were: *Arabidopsis thaliana* (*At*), *Capsella rubella* (*Cr*), *Prunus persica* (*Pp*), *Solanum lycopersicum* (*Sl*), *Aquilegia coerula* (*Ac*), *Oryza sativa* (*Os*), *Sorghum bicolor* (*Sb*), *Amborella trichopoda* (*Atr*), and *Marchantia polymorpha* (*Mp*). Numbers of phospho-sites in the meme figures represent the position of the amino acid in RBOHD from *Arabdiopsis thaliana*. Arrows indicate the position of the phospho-site (S or T) or corresponding amino acid.

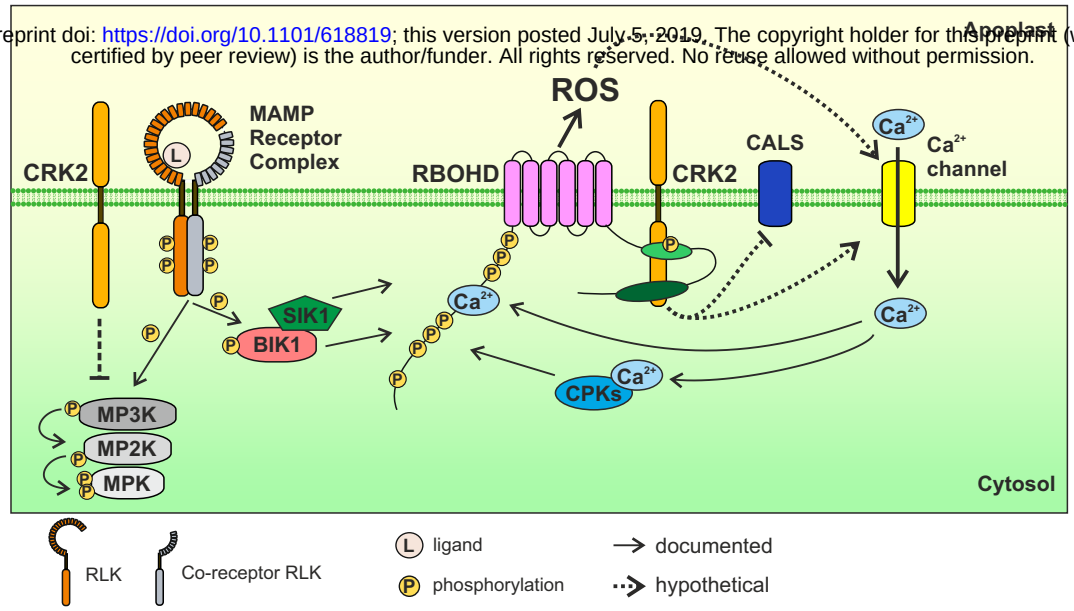

Fig. 8 Schematic model for MAMP-triggered RBOHD activation.

MAMPs are recognized by MAMP receptor complexes. RBOHD N-terminus is phosphorylated by BIK1 and SIK1 and apoplastic ROS production is induced. Apoplastic ROS production by RBOHD leads to Ca^{2+} influx into the cytosol. Ca^{2+}-binding to RBOHD N-terminus and to CPKs leads to Ca^{2+}-dependent activation of RBOHD. We found that CRK2 also contributes to the activation of RBOHD *via* phosphorylation of its C-terminus at S703. CRK2 can also mediates inhibition of MAPK activation and callose deposition *via* CALS after MAMP perception. MPK, mitogen-activated protein kinase; MP2K, MPKK; MP3K, MPKKK.